JGP Journal of General Physiology

ARTICLE

Polyunsaturated fatty acids produce a range of activators for heterogeneous I_{Ks} channel dysfunction

Briana M. Bohannon[1], Xiaoan Wu[1], Xiongyu Wu[2], Marta E. Perez[1], Sara I. Liin[3], and H. Peter Larsson[1]

Repolarization and termination of the ventricular cardiac action potential is highly dependent on the activation of the slow delayed-rectifier potassium I_{Ks} channel. Disruption of the I_{Ks} current leads to the most common form of congenital long QT syndrome (LQTS), a disease that predisposes patients to ventricular arrhythmias and sudden cardiac death. We previously demonstrated that polyunsaturated fatty acid (PUFA) analogues increase outward K^+ current in wild type and LQTS-causing mutant I_{Ks} channels. Our group has also demonstrated the necessity of a negatively charged PUFA head group for potent activation of the I_{Ks} channel through electrostatic interactions with the voltage-sensing and pore domains. Here, we test whether the efficacy of the PUFAs can be tuned by the presence of different functional groups in the PUFA head, thereby altering the electrostatic interactions of the PUFA head group with the voltage sensor or the pore. We show that PUFA analogues with taurine and cysteic head groups produced the most potent activation of I_{Ks} channels, largely by shifting the voltage dependence of activation. In comparison, the effect on voltage dependence of PUFA analogues with glycine and aspartate head groups was half that of the taurine and cysteic head groups, whereas the effect on maximal conductance was similar. Increasing the number of potentially negatively charged moieties did not enhance the effects of the PUFA on the I_{Ks} channel. Our results show that one can tune the efficacy of PUFAs on I_{Ks} channels by altering the pK_a of the PUFA head group. Different PUFAs with different efficacy on I_{Ks} channels could be developed into more personalized treatments for LQTS patients with a varying degree of I_{Ks} channel dysfunction.

Introduction

The ventricular cardiac action potential is controlled by the activation of depolarizing and repolarizing ionic currents. One of the dominant repolarizing currents during the ventricular action potential is the slow delayed-rectifier potassium current (I_{Ks}), which is critical for the timing of action potential termination (Barhanin et al., 1996; Sanguinetti et al., 1996; Salata et al., 1996). Ion channel mutations, or channelopathies, are the root of many pathological conditions, including the arrhythmogenic disorder long QT syndrome (LQTS; Bohnen et al., 2017; Alders and Christiaans, 2003; Schwartz et al., 2012). LQTS is an inherited disorder that is characterized by a prolonged QT interval—the time between ventricular depolarization and repolarization—on the electrocardiogram (Schwartz et al., 2012; Waddell-Smith and Skinner, 2016). LQTS-causing channelopathies have been discovered in many different channels, including voltage-gated Na^+ channels, Ca^{2+} channels, and K^+ channels (Alders and Christiaans, 2003; Bohnen et al., 2017; Drum et al., 2014; Harmer et al., 2010; Rivolta et al., 2002). However, the most common form of LQTS (LQT1) is caused by mutations in the voltage-gated K^+ channel known as the I_{Ks} channel.

The I_{Ks} channel underlies the slow component of the delayed-rectifier K^+ current and is composed of the voltage-gated K^+ channel, Kv7.1 α subunit, and the KCNE1 accessory β subunit (Barhanin et al., 1996; Salata et al., 1996; Sanguinetti et al., 1996). The Kv7.1 α subunit has six transmembrane-spanning segments called S1–S6 (Peroz et al., 2008; Smith et al., 2007). Segments S1–S4 make up the voltage-sensing domain, in which S4 functions as a voltage sensor due to the presence of several positively charged arginine residues (Peroz et al., 2008). Segments S5 and S6 comprise the pore domain. When the membrane becomes depolarized, the S4 segment moves outward, leading to a conformational change that allows the pore to open and K^+ ions to flow outward. Kv7.1 forms a macromolecular complex with the β subunit KCNE1, which dramatically alters the voltage dependence and kinetics of Kv7.1 channel activation, to generate the physiological I_{Ks} current (Barhanin et al., 1996; Salata et al., 1996; Sanguinetti et al., 1996; Barro-Soria et al., 2014; Osteen et al., 2010).

[1]Department of Physiology and Biophysics, Miller School of Medicine, University of Miami, Miami, FL; [2]Department of Physics, Chemistry and Biology, Linköping University, Linköping, Sweden; [3]Department of Clinical and Experimental Medicine, Linköping University, Linköping, Sweden.

Correspondence to H. Peter Larsson: plarsson@med.miami.edu.

https://doi.org/10.1085/jgp.201912396

Loss-of-function mutations in the cardiac I_{Ks} channel that lead to LQT1 result in reduced repolarizing I_{Ks} current and, as a result, prolongation of the ventricular action potential. LQT1 is particularly dangerous because it predisposes individuals to torsades de pointes, which can lead to ventricular fibrillation and sudden cardiac death (Bohnen et al., 2017). Entry into cardiac arrhythmia in patients with LQT1 is often triggered by β-adrenergic stimulation, whether by exercise or intense emotional stress (Bohnen et al., 2017; Schwartz, et al., 2012; Wu et al., 2016). Treatment options for LQTS include pharmacological attenuation of β-adrenergic stimulation by β blockers or the implantation of a cardioverter defibrillator (Schwartz et al., 2012; Cho, 2016; Waddell-Smith and Skinner, 2016). Though these treatments help to prevent arrhythmia or stop arrhythmia, they do not work for all individuals (Chockalingam et al., 2012; Schwartz et al., 2012), and they do not directly target the underlying channelopathies that lead to LQTS (Schwartz et al., 2017). Therefore, there is a need for new therapeutics that directly target the channelopathies that lead to LQTS.

We previously showed that the activity of the I_{Ks} channel can be modified by lipids, such as polyunsaturated fatty acids (PUFAs; Liin et al., 2015, 2016). PUFAs and PUFA analogues are amphipathic molecules that have two distinct structural regions that can participate in interactions with membrane proteins: (1) a charged hydrophilic head group, and (2) a long hydrophobic tail with two or more double bonds. PUFAs and PUFA analogues influence the activation of K^+ channels through a lipoelectric mechanism in which the hydrophobic tail integrates into the cell membrane near the voltage-sensing domain and electrostatically attracts the positively charged S4 through its negatively charged hydrophilic head group, thus facilitating channel activation (Fig. 1, A and B). We recently demonstrated that in PUFAs with a carboxyl head group, the position of the double bonds in the tail correlates significantly with apparent binding affinity to the I_{Ks} channel (Bohannon et al., 2019). Specifically, having the first double bond close to the carboxyl head group is important for high apparent binding affinity for the I_{Ks} channel and PUFA-induced enhancement of I_{Ks} current (Bohannon et al., 2019). It is known that a negatively charged head group is necessary for activation of voltage-gated K^+ channels (Liin et al., 2015; Börjesson et al., 2008). Docosahexaenoic acid (DHA), which can bear a negative charge at its carboxyl head group, shifts the voltage dependence of Kv7.1 channel activation to more negative voltages; however, coexpression of KCNE1 abolishes DHA sensitivity (Liin et al., 2015). KCNE1 was recently shown to tune PUFA sensitivity by inducing a conformational change of the S5-P-helix loop that results in protonation of the PUFA head group (Larsson et al., 2018). This protonation can be circumvented by using PUFA analogues that are negatively charged at physiological pH (pH 7.4), such as DHA-glycine or N-arachidonoyl taurine (Liin et al., 2015, 2016). In addition to an electrostatic effect on the voltage sensor of the I_{Ks} channel, our group also recently demonstrated that PUFA analogues have an additional effect on the pore of the I_{Ks} channel (Liin et al., 2018): A lysine residue (K326) in the S6 helix of the I_{Ks} channel electrostatically interacts with the negatively charged head group of PUFA analogues, and this electrostatic interaction increases the maximal conductance (G_{max}) of the cardiac I_{Ks} channel (Liin et al., 2018; Fig. 1, B–D).

A thorough characterization of PUFA analogues with a wide range of effects on the cardiac I_{Ks} channel provides a means to develop novel treatments for LQT1-causing mutations of different severity. LQT1 is variable in its severity and can present with different symptoms based on the individual (Schwartz et al., 2012). For example, some patients carrying a mutation in KCNQ1 can have milder phenotypes associated with less severe prolongation of the QT interval (Schwartz et al., 2012; Wu et al., 2016; Amin et al., 2012; Chouabe et al., 2000). For example, R533W, which causes a positive shift of ∼15 mV in the voltage dependence of activation, is associated with a milder cardiac phenotype (Chouabe et al., 2000). In other cases, such as for the KCNQ1 mutation A341V, that is one of the most severe presentations of LQT1; >30% of patients experience cardiac arrest or sudden cardiac death (Crotti et al., 2007; Schwartz et al., 2012). These examples highlight extreme differences in the manifestation of LQT1 in the clinical population that occur in a mutation-specific manner. Treatment for such distinct phenotypes requires an individualized approach. For this reason, there is a need to find new ways in which the effects of PUFA analogues can be tuned, allowing for more personalized treatment options for patients with LQT1. The purpose of the present study was to evaluate different PUFA head groups to determine if the activating effects of PUFA analogues can be enhanced or attenuated through modifications to the charged PUFA head group.

Materials and methods

Molecular biology

Kv7.1 and KCNE1 channel complementary RNA were transcribed using the mMessage mMachine T7 kit (Ambion). 50 ng of complementary RNA was injected at a 3:1, weight/weight (Kv7.1/KCNE1) ratio into defolliculated *Xenopus laevis* oocytes (Ecocyte) for I_{Ks} channel expression. Site-directed mutagenesis was performed using the Quickchange II XL Mutagenesis Kit (QIAGEN Sciences) for mutations in the Kv7.1 α subunit. Injected cells were incubated for 72–96 h in standard ND96 solution (96 mM NaCl, 2 mM KCl, 1 mM $MgCl_2$, 1.8 mM $CaCl_2$, and 5 mM HEPES; pH 7.5) containing 1 mM pyruvate at 16°C before electrophysiological recordings.

Two-electrode voltage clamp

X. laevis oocytes were recorded in the two-electrode voltage-clamp configuration. Recording pipettes were filled with 3 M KCl. The chamber was filled with ND96 recording solution (96 mM NaCl, 2 mM KCl, 1 mM $MgCl_2$, 1.8 mM $CaCl_2$, and 5 mM Tricine; pH 9.0 or 96 mM NaCl, 2 mM KCl, 1 mM $MgCl_2$, 1.8 mM $CaCl_2$, and 5 mM HEPES; pH 7.5). PUFAs were obtained from Cayman Chemical or were synthesized in-house (University of Linköping) and kept at −20°C as 100-mM stock solutions in ethanol. Serial dilutions of the different PUFAs were prepared from stocks to make 0.2-, 0.7-, 2-, 7-, 20-, and 70-µM concentrations in ND96 solutions (ND96 recording solutions were made at both pH 7.5 and pH 9.0). PUFAs were perfused into the

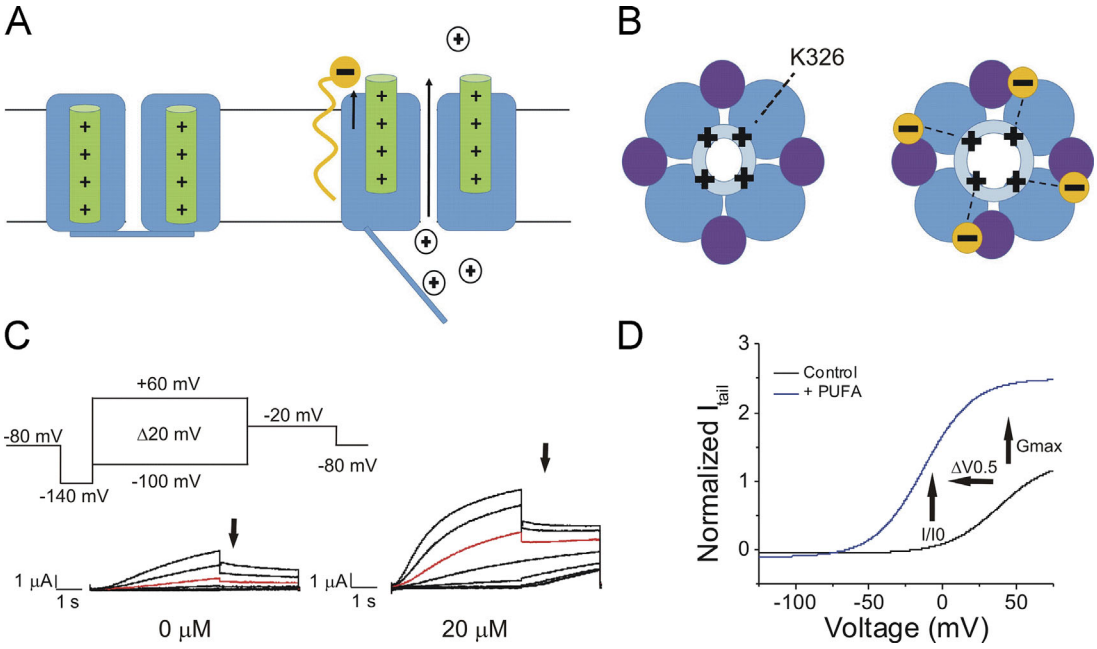

Figure 1. **Illustration of the lipoelectric mechanism and measured effects on the cardiac I_{Ks} channel. (A)** Schematic side view (left) of the I_{Ks} channel with S4 in green. Illustration (right) of the electrostatic interaction of a PUFA analogue (orange) with the voltage sensor (green) of the cardiac I_{Ks} channel, which leads to potentiation of upward S4 movement. **(B)** Schematic top view (left) of the I_{Ks} channel with Kv7.1 in blue (light blue, pore domain; dark blue, voltage-sensing domain) and KCNE1 in purple. Illustration (right) of the electrostatic interaction of a PUFA analogue (orange) with the positively charged lysine residue K326 in the S6 segment of the cardiac I_{Ks} channel, which leads to an increase in the G_{max} of the I_{Ks} channel. **(C)** Activation protocol for the cardiac I_{Ks} channel using two-electrode voltage clamp and raw current traces in 0 μM PUFA analogue (left) and 20 μM PUFA analogue (right), with arrows indicating tail currents. Red trace occurs at 20 mV for visualization of PUFA-induced increases in current. **(D)** Representative current versus voltage relationship in 0 μM (black line) and 20 μM PUFA (blue line) highlighting an increase in I/I_0 at 0 mV, leftward shift in the $V_{0.5}$, and increase in G_{max} denoted by arrows.

recording chamber using the Rainin Dynamax Peristaltic Pump (Model RP-1). Combinations of PUFA analogues, monounsaturated fatty acids (MUFAs), saturated fatty acids (SFAs), and albumin (A7906-10G; Sigma-Aldrich) were applied to emulate physiological circulation of fatty acids in the human body. We applied the PUFA analogue linoleoyl glycine (lin-glycine; 0.2 mM), the MUFA oleic acid (0.2 mM), and the SFA stearic acid (0.2 mM) in combination with albumin (0.1 mM) to estimate the effect of physiological levels of PUFAs on I_{Ks} channels in the presence of physiological levels of the fatty acid–binding protein albumin and other fatty acids in interstitial space (Abdelmagid et al., 2015; Tsukamoto and Sugawara, 2018).

Electrophysiological recordings were obtained using Clampex 10.3 software (Axon, pClamp; Molecular Devices). During the application of PUFAs, the membrane potential was stepped every 30 s from −80 mV to 0 mV for 5 s before stepping to −40 mV and back to −80 mV. The application protocol was used to ensure that the PUFA effects reached steady state. The PUFA effects reached steady state in 10 min when applied at the highest concentrations (7 and 20 μM). A voltage-step protocol (Fig. 1 C, inset) was used to measure the current versus voltage (I-V) relationship before PUFA application and after the PUFA effects had reached steady state for each concentration of PUFA. During the activation protocol, cells were held at −80 mV followed by a hyperpolarizing prepulse to −140 mV. The voltage was then stepped from −100 to 60 mV (Δ20 mV) followed by a voltage step to −20 mV to measure tail currents. Following the test pulse to measure tail currents (Fig. 1 C, arrows), cells were held again at −80 mV.

Data analysis

Tail currents were analyzed using Clampfit 10.3 software in order to obtain conductance versus voltage (G-V) curves to determine the voltage dependence of channel activation. The $V_{0.5}$, the voltage at which half the maximal tail current occurs, was obtained by fitting the G-V curves from each concentration of PUFA with a Boltzmann equation (Fig. 1 D):

$$G(V) = \frac{Gmax}{1 + e^{(V_{0.5} - V)/s}},$$

where G_{max} is the maximal conductance at positive voltages and s is the slope factor in millivolts. The current values for each concentration at 0 mV were used to plot the dose–response curves for each PUFA. Dose–response curves were fit using the Hill equation in order to obtain the K_m value for each PUFA:

$$\frac{I}{I_0} = 1 + \frac{A}{1 + \frac{Km^n}{x^n}},$$

where A is the relative increase in current ($\Delta I/I_0$) caused by the PUFA at saturating concentrations, K_m is the apparent affinity of the PUFA, x is the concentration, and n is the Hill coefficient. In some cases, there was variability in the $V_{0.5}$ between batches of oocytes. To correct for variability between batches of oocytes, we applied a correction to compensate for a $V_{0.5}$ that differs

greatly from 20 mV (the typical $V_{0.5}$ for the I_{Ks} channel). This allowed us to more consistently measure PUFA-induced I_{Ks} current increases. In our correction, we subtracted the $V_{0.5}$ (obtained from using the Boltzmann equation) by 20 mV and used the current measured at the resulting voltage. The G_{max} for each concentration was obtained from the fitted values given by the Boltzmann fit and then normalized to the G_{max} in control solution (0 µM), G_{max0}. All data is given as mean ± SEM. Graphs plotting mean and SEM for I/I_0, $\Delta V_{0.5}$, G_{max}, and K_m were generated using Origin 9 software. PUFA artwork was made using CorelDRAW Software. To determine if there were significant differences between PUFA-induced effects on I/I_0, $\Delta V_{0.5}$, and G_{max}, we conducted one-way ANOVA followed by Tukey's honestly significant difference test (HSD) for multiple comparisons. For data in which dose–response curves were well fitted, we used the fitted max values and K_m for the statistical tests. For data in which dose–response curves were not clearly reaching saturation, we used the values at 20 µM for the statistical tests. Significance α-level was set at $P < 0.05$; asterisks denote significance: *, $P < 0.05$; **, $P < 0.01$; ***, $P < 0.001$; and ****, $P < 0.0001$.

Estimated pK_a values

pK_a, the negative log of the acid dissociation constant, values of PUFA analogues in solution were calculated using Marvin Software (ChemAxon). However, studies of PUFAs in lipid bilayers and our previous studies on PUFA–I_{Ks} channel interactions showed that there is a large difference in the pK_a values in solution (calculated according to the structure) compared with the measured pK_a of PUFAs in the lipid bilayer (Börjesson and Elinder, 2011; Elinder and Liin, 2017) and in close contact with the I_{Ks} channel (Elinder and Liin, 2017; Liin et al., 2015). The average difference between the calculated solution pK_a values and experimental found pK_a values for PUFAs associated with I_{Ks} channels is ∼3.5 (Liin et al., 2015). We therefore added this correction factor to the calculated solution pK_a values to generate our estimated pK_a value for PUFAs associated with the I_{Ks} channel.

Hierarchical cluster analysis

Hierarchical cluster analysis was performed using BioVinci data visualization software (BioTuring). Effects on I/I_0, $\Delta V_{0.5}$, and G_{max} at 20 µM were normalized to the PUFA analogue with the largest influence on each of the three effects so that these effects were now scaled from 0.0 to 1.0, 1.0 being the largest effect. Each parameter (I/I_0, $\Delta V_{0.5}$, and G_{max}) was then used as input for clustering to generate the dendrogram and heat map.

Online supplemental material

Specific synthesis pathways for PUFA analogues that were synthesized in-house are described in detail in the Supplemental materials and methods. Fig. S1 contains data on the current versus voltage relationship between pH 7.5 and pH 9.0. Fig. S2 shows that reduction of I_{Ks} current by the application of DHA-taurine is not intrinsically related to the taurine head group alone. Fig. S3 shows that residues in the voltage sensor and pore are important for electrostatic activation of the cardiac I_{Ks} channel. Fig. S4 contains effects of lin-AP3 on I_{Ks} activation at pH 9.0.

Results

Linoleoyl-taurine (lin-taurine) and lin-glycine increased the I_{Ks} current by differentially affecting the $V_{0.5}$ and the G_{max}

We previously demonstrated that the negative charge of a PUFA with a carboxyl head group is neutralized by the presence of KCNE1 in I_{Ks} channels (Larsson et al., 2018). For this reason, PUFAs with a carboxyl head group tend to have little effect on I_{Ks} channel activation at physiological pH. In this study, we investigated the effects of other head groups that are expected to promote I_{Ks} channel activation through the lipoelectric mechanism (Fig. 1, A and B) with effects on the voltage sensor (Fig. 1 A) and the pore (Fig. 1 B). We compared the effects between PUFAs with varying functional groups of the hydrophilic PUFA head but with the same hydrocarbon tail. To do this, we used a two-electrode voltage clamp and a series of depolarizing voltage steps to measure the effects of PUFAs on I_{Ks} current (Fig. 1 C). This allowed us to measure the effects on the normalized current at 0 mV (I/I_0), the shift in voltage dependence of I_{Ks} channel activation ($\Delta V_{0.5}$), and the G_{max} (Fig. 1 D).

We first compared three PUFAs and PUFA analogues that have a linoleic acid tail: linoleic acid, lin-glycine, and lin-taurine (Fig. 2, A–C). Application of 20 µM linoleic acid (Fig. 2 A), which has a carboxyl head group, did not increase in I/I_0 (0.5 ± 0.1; Fig. 2 D), did not left-shift the $V_{0.5}$ of I_{Ks} channel activation (4.7 ± 0.9 mV; Fig. 2 F), and did not increase the G_{max} (0.7 ± 0.1; Fig. 2 H). Lin-glycine, when applied at 20 µM (Fig. 2 B), produced a moderate increase in I/I_0 (5.3 ± 0.5; Fig. 2 D) and a moderate shift in the $V_{0.5}$ (−26.4 ± 4.4 mV; Fig. 2 F) and produced the largest increase in the G_{max} (2.4 ± 0.2; Fig. 2 H). Lin-taurine, when applied at 20 µM (Fig. 2 C), produced the largest increase in I/I_0 (10.4 ± 4.0; Fig. 2 D) and the largest left-shift in the $V_{0.5}$ (−73.1 ± 2.6 mV; Fig. 2 F) and increased the G_{max} (2.0 ± 0.6; Fig. 2 H). Statistical analysis of the fitted parameters of the dose–response curves show that lin-taurine had the biggest increase in I/I_0 (Fig. 2 E) and $V_{0.5}$ (Fig. 2 G), whereas lin-glycine had the biggest increase in G_{max} (Fig. 2 I). The size of the voltage shifts caused by the three PUFAs correlates with the predicted protonation (i.e., charge) of the different head groups (from the pK_a values estimated for carboxyl, glycine, and taurine head groups in the lipid bilayer) at physiological pH (Table 1). In contrast, the effects on G_{max} did not correlate with the predicted charge of the PUFA head groups.

The different effects of lin-glycine and lin-taurine on the $V_{0.5}$ were not due to differences in the lengths of the PUFA head groups

One structural difference between the head groups of lin-glycine and lin-taurine was that the glycine group was shorter in length than the taurine group (Fig. 2, B and C). Therefore, we explored whether the different lengths of the head groups could explain the different activating effects of the two PUFAs on the I_{Ks}

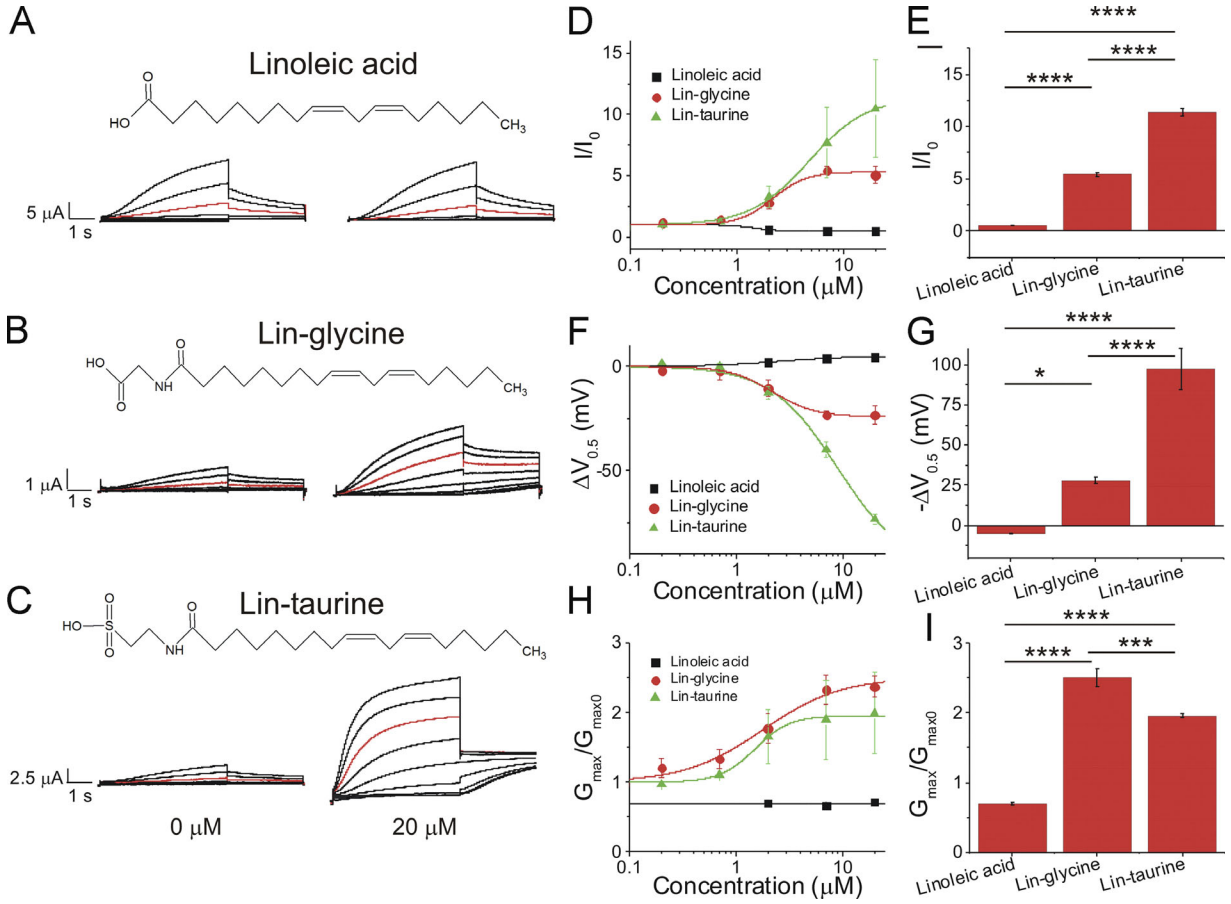

Figure 2. **Lin-taurine produces the most potent activation of the I_{Ks} channel compared with lin-glycine and linoleic acid. (A–C)** Structure of and raw current traces measured in 0 μM (left) and 20 μM (right) (A) linoleic acid, (B) lin-glycine, and (C) lin-taurine. Red trace shows currents at 20 mV for visualization of PUFA-induced effects on current. **(D)** Dose-dependent effects of linoleic acid (n = 5), lin-glycine (n = 4), and lin-taurine (n = 3) on I_{Ks} current (I/I_0; mean ± SEM at maximal concentration). **(E)** Statistical differences on I/I_0 effects (I/I_0 fitted from the dose–response curve) measured by one-way ANOVA followed by Tukey's HSD post hoc analysis. **(F)** Dose-dependent effects of linoleic acid, lin-glycine, and lin-taurine on I_{Ks} voltage dependence ($\Delta V_{0.5}$). **(G)** Statistical differences on $\Delta V_{0.5}$ effects ($\Delta V_{0.5}$ fitted from the dose–response curve) measured by one-way ANOVA followed by Tukey's HSD post hoc analysis. **(H)** Dose-dependent effects of linoleic acid, lin-glycine, and lin-taurine on I_{Ks} G_{max}. **(I)** Statistical differences on G_{max} effects (G_{max} fitted from the dose–response curve) measured by one-way ANOVA followed by Tukey's HSD post hoc analysis. *, P < 0.05; ***, P < 0.001; ****, P < 0.0001.

channel. To do so, we inserted additional carbons into the head group of lin-glycine to elongate the glycine head group and then compared the effects of lin-glycine, lin-glycine+1C (Fig. 3 A), and lin-glycine+2C (Fig. 3 B). With the insertion of one additional carbon in the glycine head group, lin-glycine+1C had a similar length as lin-taurine. Application of lin-glycine produced an increase in I/I_0 (5.3 ± 0.5), whereas lin-glycine+1C and +2C surprisingly produced a smaller increase in I/I_0 (1.7 ± 0.1 and 1.6 ± 0.1, respectively; Fig. 3, C and I). In addition, lin-glycine produced the largest shift in the $V_{0.5}$ (−26.4 ± 4.4 mV) compared with lin-glycine+1C (−7.2 ± 2.5 mV) and lin-glycine+2C (−8.7 ± 0.5 mV; Fig. 3, D and J). Lin-glycine increased the G_{max} of the I_{Ks} channel (2.4 ± 0.2), whereas lin-glycine+1C and lin-glycine+2C produced no change in the G_{max} (1 ± 0.1 and 0.9 ± 0.1, respectively; Fig. 3, E and K).

One possible mechanism behind the decreased effects of lin-glycine+1C and lin-glycine+2C compared with lin-glycine is that the addition of carbons in the glycine head group shifts the pK_a of the head group, which thereby promotes protonation and loss of the negative charge in the head group. We therefore repeated the experiments with lin-glycine, lin-glycine+1C, and lin-glycine+2C at pH 9.0. Using PUFAs with a carboxyl head group, we previously demonstrated that conducting experiments at pH 9.0 can deprotonate the head group to restore its negative charge and allow PUFAs to activate the I_{Ks} channel (Bohannon et al., 2018; Liin et al., 2015). Changing the solution from pH 7.5 to pH 9.0 did not alter the normal activation of the I_{Ks} channel (Fig. S1). At pH 9.0, lin-glycine, lin-glycine+1C, and lin-glycine+2C all produced a similar left-shift in the voltage dependence of I_{Ks} channel activation at 20 μM (−43.6 ± 1.6 mV, −41.7 ± 1.7 mV, and −47.9 ± 2.4 mV, respectively; Fig. 3, G and J). Note that at pH 9.0, application of lin-glycine resulted in a larger left-shift in the voltage dependence of the I_{Ks} channel compared with the left-shifting effect of lin-glycine at pH 7.5 (Fig. 3 J). This is consistent with our estimated pK_a = 7.6 for lin-glycine: At pH 7.5, 50% of lin-glycine was negatively charged, whereas at pH 9.0, lin-glycine was almost fully in its deprotonated and negatively charged form. Lin-glycine displayed higher apparent

Table 1. **PUFAs/PUFA analogues and their estimated pK_a values**

PUFA	pK_{a1}	pK_{a2}	pK_{a3}
Linoleic acid	8.5	NA	NA
Lin-glycine	7.6	NA	NA
Lin-taurine	2.7	NA	NA
Lin-glycine+1C	8.0	NA	NA
Lin-glycine+2C	8.0	NA	NA
Lin-aspartate	7.6	9.1	NA
Lin-cysteic acid	2.6	7.1	NA
Lin-AP3	5.0	7.7	11.8
DHA	8.3	NA	NA
DHA-glycine	7.5	NA	NA
DHA-taurine	2.8	NA	NA
Pinolenic acid	8.4	NA	NA
Pin-glycine	7.5	NA	NA
Pin-taurine	2.8	NA	NA

Estimated pK_a values for PUFAs and PUFA analogues associated with the cardiac I_{Ks} channel were calculated by adding a factor of 3.5 to the starting pK_a value calculated in solution.

affinity and began to shift the $V_{0.5}$ at lower concentrations compared with lin-glycine+1C and lin-glycine+2C (Fig. 3 G). Although the left-shifting effects of lin-glycine, lin-glycine+1C, and lin-glycine+2C were improved at pH 9.0 (Fig. 3, G and J), all three PUFA analogues decreased the G_{max} of the channel (0.6 ± 0.1, 0.9 ± 0.1, and 0.5 ± 0.1, respectively) at pH 9.0 (Fig. 3, H and K). The reason for this decrease in G_{max} is unclear. At pH 9.0, lin-glycine, lin-glycine+1C, and lin-glycine+2C all increased I/I_0 (2.3 ± 0.1, 2.7 ± 0.3, and 1.8 ± 0.04, respectively; Fig. 3, F and I).

The finding that the voltage-shifting effects of lin-glycine+1C and lin-glycine+2C are similar to that of lin-glycine at pH 9.0 but smaller at pH 7.5 suggests that the addition of one and two additional carbons in the glycine head group shifts the pK_a of the glycine head group and reduces the likelihood that the glycine head will be deprotonated and negatively charged at pH 7.5. The size of the voltage shifts for lin-glycine+1C and lin-glycine+2C at pH 7.5 (50% smaller than for lin-glycine) is consistent with our estimated pK_a values of lin-glycine+1C and lin-glycine+2C, which are both ∼8.0 compared with 7.6 for lin-glycine (Table 1). That the voltage-shifting effects of lin-glycine, lin-glycine+1C, and lin-glycine+2C at pH 9.0 are all similar suggests that is it not the length of the head group that renders lin-taurine more effective that lin-glycine but mainly the protonation state of the PUFA head groups.

Increasing the number of potentially charged moieties on the PUFA head group did not further promote I_{Ks} channel activation

Because we previously found that the charge of the head group is important for activating the cardiac I_{Ks} channel, we tested whether it is possible to further improve the activating effects of PUFA analogues by increasing the charge available on the PUFA head group. To do so, we compared PUFA analogues that have one possible charge (lin-taurine and lin-glycine), two possible charges (linoleoyl-aspartate [lin-aspartate] and linoleoyl-cysteic acid [lin-cysteic acid]; Fig. 4, A and B), and three possible charges (lin-AP3; Fig. 4 C). Interestingly, increasing the number of potentially negatively charged groups on the PUFA head group did not further improve the effects on I/I_0, $V_{0.5}$, or G_{max}. Lin-aspartate, which has two potentially charged moieties, moderately increased I/I_0 (4.0 ± 0.1; Fig. 4 D), moderately left-shifted the $V_{0.5}$ (−34.5 ± 2.3 mV; Fig. 4 E), and moderately increased G_{max} (1.4 ± 0.1; Fig. 4 F). The effects of lin-aspartate were similar to the effects of lin-glycine, which has only one potentially charged moiety (Fig. 4, G–I). Lin-cysteic acid (Fig. 4 C), which also possesses two potentially charged moieties, substantially increased I/I_0 (9.2 ± 0.4; Fig. 4 D), substantially left-shifted the $V_{0.5}$ of I_{Ks} channel activation (−58.4 ± 2.8 mV; Fig. 4 E), and substantially increased the G_{max} (2.0 ± 0.2; Fig. 4 F). The effects of lin-cysteic acid were similar to the effects of lin-taurine, which has only one potentially charged moiety (Fig. 4, G–I). Lastly, lin-AP3, which has three potential negative charges, produced the smallest increase in I/I_0 (1.8 ± 0.3; Fig. 4, D and G) and the smallest left-shift in the $V_{0.5}$ (−5.7 ± 1.3 mV; Fig. 4, E and H) and produced no change in the G_{max} (1.1 ± 0.1; Fig. 4, F and I). Together, these data show that having more than one potentially charged moiety of the head group does not necessarily improve the efficacy of PUFA analogues, leading us to concentrate on glycine and taurine head groups as potential therapeutics for LQTS.

Taurine compounds had the largest current increase and left-shifting effect on the I_{Ks} channel

We next compared PUFAs and PUFA analogues that have a DHA or pinolenic acid tail group to determine if the efficacy of glycine and taurine head groups are consistent across PUFA tail groups. DHA, which has a carboxyl head group, produced little change in I_{Ks} current at 20 µM (Fig. 5 A) and produced a slight increase in I/I_0 (2.0 ± 0.6; Fig. 5 D). DHA-glycine, which has a glycine head group, produced a larger increase in I/I_0 (4.7 ± 1.3 at 20 µM) relative to DHA. DHA-taurine produced the most robust increases in I_{Ks} current at 7 µM compared with PUFA analogues with a DHA tail, increasing I/I_0 by 5.1 ± 0.7 at 7 µM (Fig. 5 D). Surprisingly, at concentrations >7 µM (20 µM), DHA-taurine decreased the current for reasons that are unclear. For this reason, we report the effects observed at 7 µM. When the effects on the $V_{0.5}$ of the I_{Ks} channel were measured, DHA did not left-shift the $V_{0.5}$ (0.1 ± 1.4 mV; Fig. 5 F), DHA-glycine had a moderate left-shifting effect (−16.5 ± 1.3 mV at 20 µM), and DHA-taurine had a more robust left-shifting effect (−45.3 ± 2.9 mV at 7 µM; Fig. 5 F). DHA, DHA-glycine, and DHA-taurine all increased the G_{max} (1.7 ± 0.3 at 20 µM, 2.0 ± 0.2 at 20 µM, and 1.7 ± 0.1 at 7 µM, respectively; Fig. 5 H). Statistical analysis of the fitted parameters of the dose–response curves show that DHA-taurine had the biggest increase in the $V_{0.5}$ (Fig. 5 G), whereas DHA-glycine had the biggest increases in I/I_0 (Fig. 5 E) and G_{max} (Fig. 5 I).

Application of 20 µM pinolenic acid (Fig. 6 A), which has a carboxyl head group, increased I/I_0 slightly (1.5 ± 0.3; Fig. 6 D), had little left-shifting effect on the $V_{0.5}$ of I_{Ks} channel activation (−6 ± 1.8 mV; Fig. 6 F), and produced a slight increase in the G_{max}

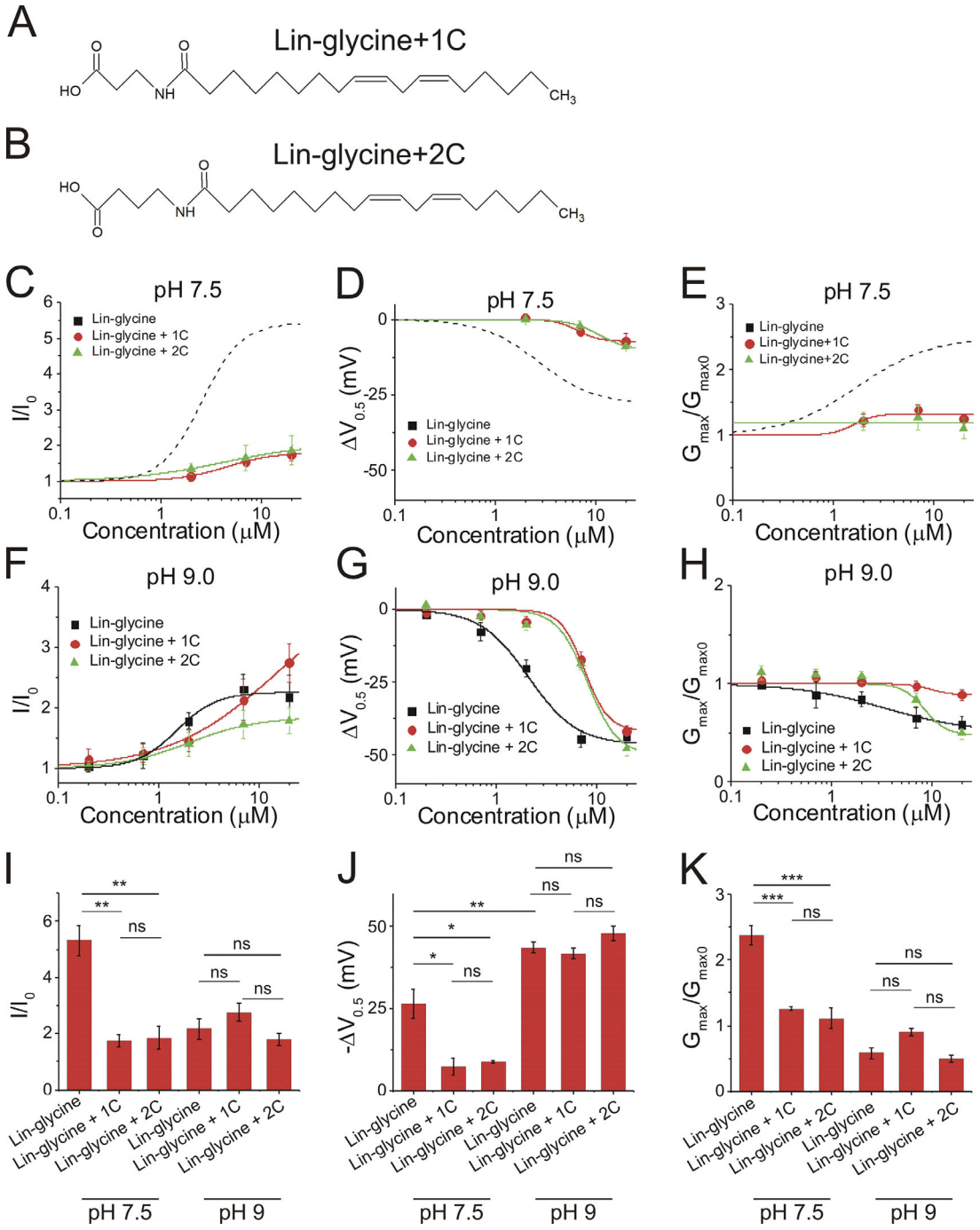

Figure 3. **Increasing the length of the lin-glycine head group alters the pK_a and reduces the activating effect on the I_{Ks} channel. (A and B)** Structure of (A) lin-glycine with the addition of one carbon in the head group (lin-glycine+1C) and (B) lin-glycine with the addition of two carbons in the head group (lin-glycine+2C). **(C–H)** Dose-dependent effects of lin-glycine (n = 4), lin-glycine+1C (n = 3), and lin-glycine+2C (n = 3) on (C) I_{Ks} current (I/I_0) at pH 7.5, (D) I_{Ks} voltage dependence ($\Delta V_{0.5}$) at pH 7.5, (E) I_{Ks} G_{max} at pH 7.5, (F) I/I_0 at pH 9.0, (G) $\Delta V_{0.5}$ at pH 9.0, and (H) G_{max} at pH 9.0 (mean ± SEM at maximal concentration). **(I–K)** Statistical differences at 20 μM on (I) I/I_0 effect, (J) $\Delta V_{0.5}$ effect, and (K) G_{max} effect measured by one-way ANOVA followed by Tukey's HSD post hoc analysis. *, P < 0.05; **, P < 0.01; ***, P < 0.001. ns, not significant.

(1.4 ± 0.2; Fig. 6 H). Application of 20 μM pinoleoyl-glycine (pin-glycine; Fig. 6 B) produced a moderate increase in I/I_0 (3.8 ± 0.2; Fig. 6 D), had a moderate left-shifting effect on the $V_{0.5}$ of I_{Ks} channel activation (−21.1 ± 2.5 mV; Fig. 6 F), and increased the G_{max} (1.8 ± 0.1; Fig. 6 H). Application of 20 μM pinoleoyl-taurine (pin-taurine; Fig. 6 C) produced a robust increase in I/I_0 (9.0 ± 1.4; Fig. 6 D), potently left-shifted the $V_{0.5}$ of I_{Ks} channel activation (−51.6 ± 3.5 mV; Fig. 6 F), and increased the G_{max} (1.9 ± 0.3; Fig. 6 H) relative to other PUFA analogues with a pinolenic acid tail. Statistical analysis of the fitted parameters of the dose–response curves show that pin-taurine had the biggest increase in I/I_0 (Fig. 6 E) and the $V_{0.5}$ (Fig. 6 G), whereas there

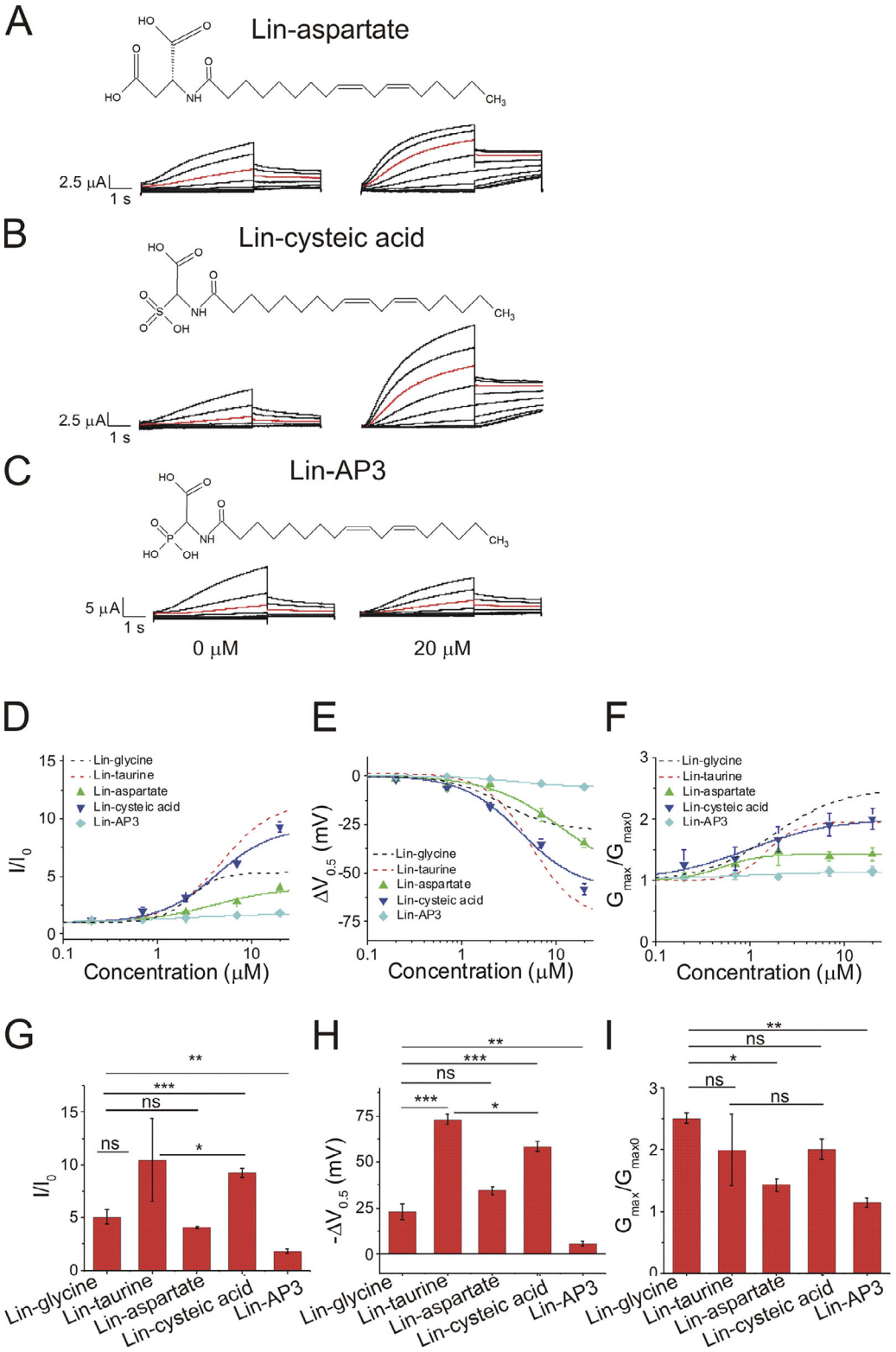

Figure 4. **Increasing the number of potentially charged moieties of the PUFA head group does not improve PUFA-induced I_{Ks} activation. (A–C)** Structure of and raw current traces measured in 0 μM (left) and 20 μM (right) (A) lin-aspartate, (B) lin-cysteic acid, and (C) lin-AP3. Red trace shows currents at 20 mV for visualization of PUFA-induced effects on current. **(D–F)** Dose-dependent effects of lin-glycine (n = 4), lin-taurine (n = 3), lin-aspartate (n = 4), lin-cysteic acid (n = 5), and lin-AP3 (n = 3) on (D) I_{Ks} current (I/I_0), (E) I_{Ks} voltage dependence ($\Delta V_{0.5}$), and (F) I_{Ks} G_{max} (mean ± SEM at maximal concentration). **(G-I)** Statistical differences at 20 μM on (G) I/I_0 effect, (H) $\Delta V_{0.5}$ effect, and (I) G_{max} effect measured by one-way ANOVA followed by Tukey's HSD post hoc analysis. *, P < 0.05; **, P < 0.01; ***, P < 0.001. ns, not significant.

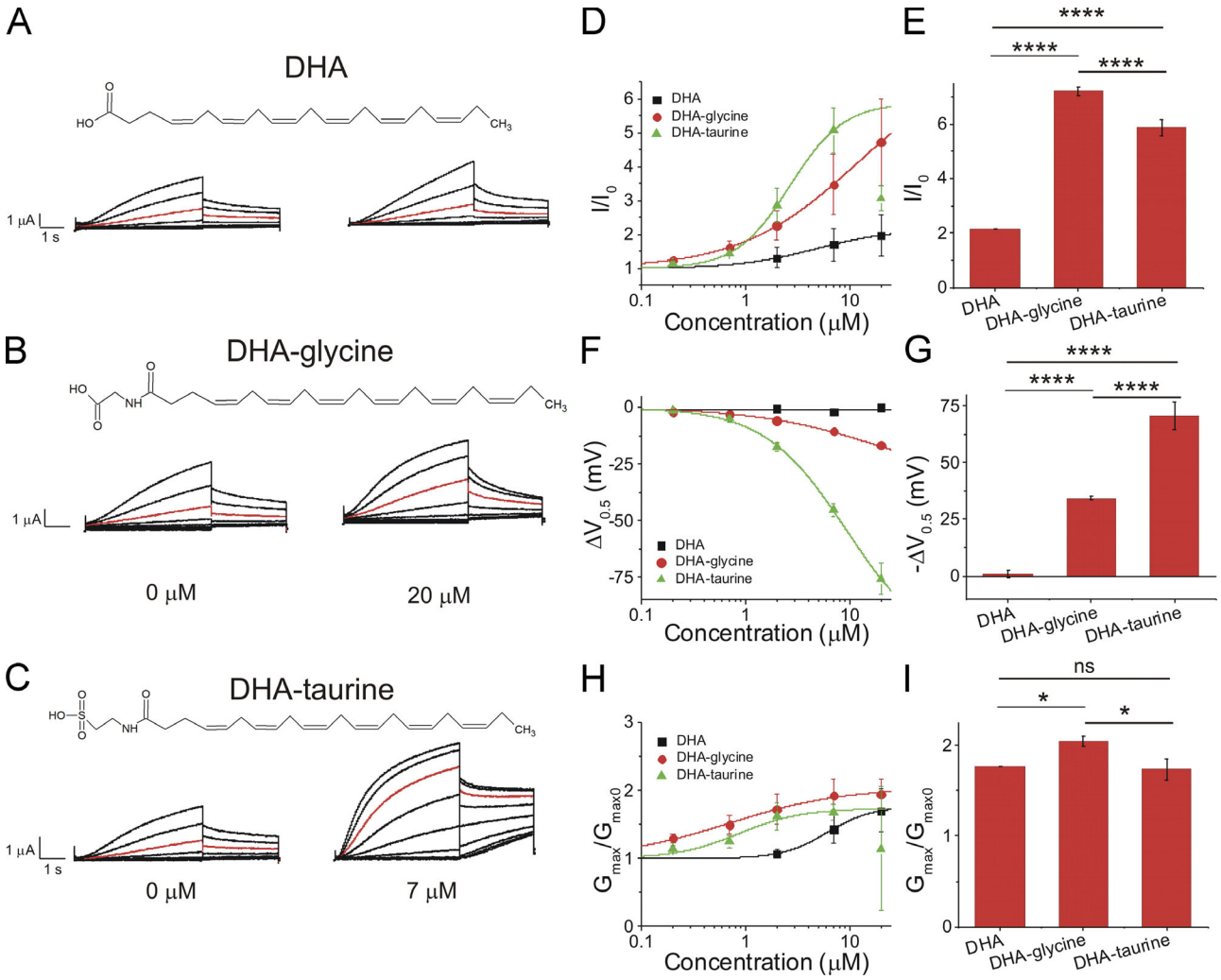

Figure 5. **DHA-taurine at 7 μM produces the most potent activation of the I_{Ks} channel compared with DHA-glycine and DHA at 20 μM. (A–C)** Structure of and raw current traces measured in 0 μM (left) and 20 μM (right) (A) DHA, (B) DHA-glycine, and (C) DHA-taurine, 0 μM (left) and 7 μM (right). We report effects of DHA-taurine at 7 μM due to an unclear reduction in current caused by the application of 20 μM. Red trace shows currents at 20 mV for visualization of PUFA-induced effects on current. **(D)** Dose-dependent effects of DHA (n = 4), DHA-glycine (n = 4), and DHA-taurine (n = 3) on I_{Ks} current (I/I_0; mean ± SEM at maximal concentration). **(E)** Statistical differences on I/I_0 effects (I/I_0 fitted from the dose–response curve) measured by one-way ANOVA followed by Tukey's HSD post hoc analysis. **(F)** Dose-dependent effects of DHA, DHA-glycine, and DHA-taurine on I_{Ks} voltage dependence ($\Delta V_{0.5}$). **(G)** Statistical differences on $\Delta V_{0.5}$ effects ($\Delta V_{0.5}$ fitted from the dose–response curve) measured by one-way ANOVA followed by Tukey's HSD post hoc analysis. **(H)** Dose-dependent effects of DHA, DHA-glycine, and DHA-taurine on I_{Ks} G_{max}. **(I)** Statistical differences on G_{max} effects (G_{max} fitted from the dose–response curve) measured by one-way ANOVA followed by Tukey's HSD post hoc analysis. *, P < 0.05; ****, P < 0.0001. ns, not significant.

were no significant differences in G_{max} among the three compounds (Fig. 6 I).

As previously mentioned, DHA-taurine produced an unexpected decrease in I/I_0 and G_{max} at 20 μM. The largest effect on G_{max} induced by DHA-taurine on the I_{Ks} channel occurred at 7 μM, followed by a drastic decrease in G_{max} at 20 μM. We also observed a similar decrease in G_{max} at 20 μM with pin-taurine; however, this decrease in G_{max} was not as pronounced as we saw with 20 μM of DHA-taurine. The source of the reduction in G_{max} with the application of some taurine compounds is not known. One possibility is that it is caused by a steric effect of the longer taurine head group, resulting in obstruction of the I_{Ks} channel pore. To determine whether the reduction in G_{max} is intrinsic to the taurine head group, we applied 100 μM taurine to the I_{Ks} channel. However, 100 μM taurine alone did not change I/I_0, $\Delta V_{0.5}$, or G_{max} (Fig. S2), suggesting that the taurine head group alone is not responsible for the reduction in G_{max}. Therefore, PUFA-induced decreases in G_{max} at concentrations ≥20 μM must be due to a different mechanism that occurs through the combination of the taurine head group and the PUFA tail.

We directly compared the effects of PUFA analogue head groups across different PUFA tails to see if there were any differences in apparent binding affinity or effects on I/I_0, $\Delta V_{0.5}$, or G_{max} depending on the tail. Our previous data and the data in this study suggest that PUFA analogues with glycine head groups have a pK_a of ∼7.5–7.6 when associated with I_{Ks} channels, suggesting that half the PUFA molecules with a glycine

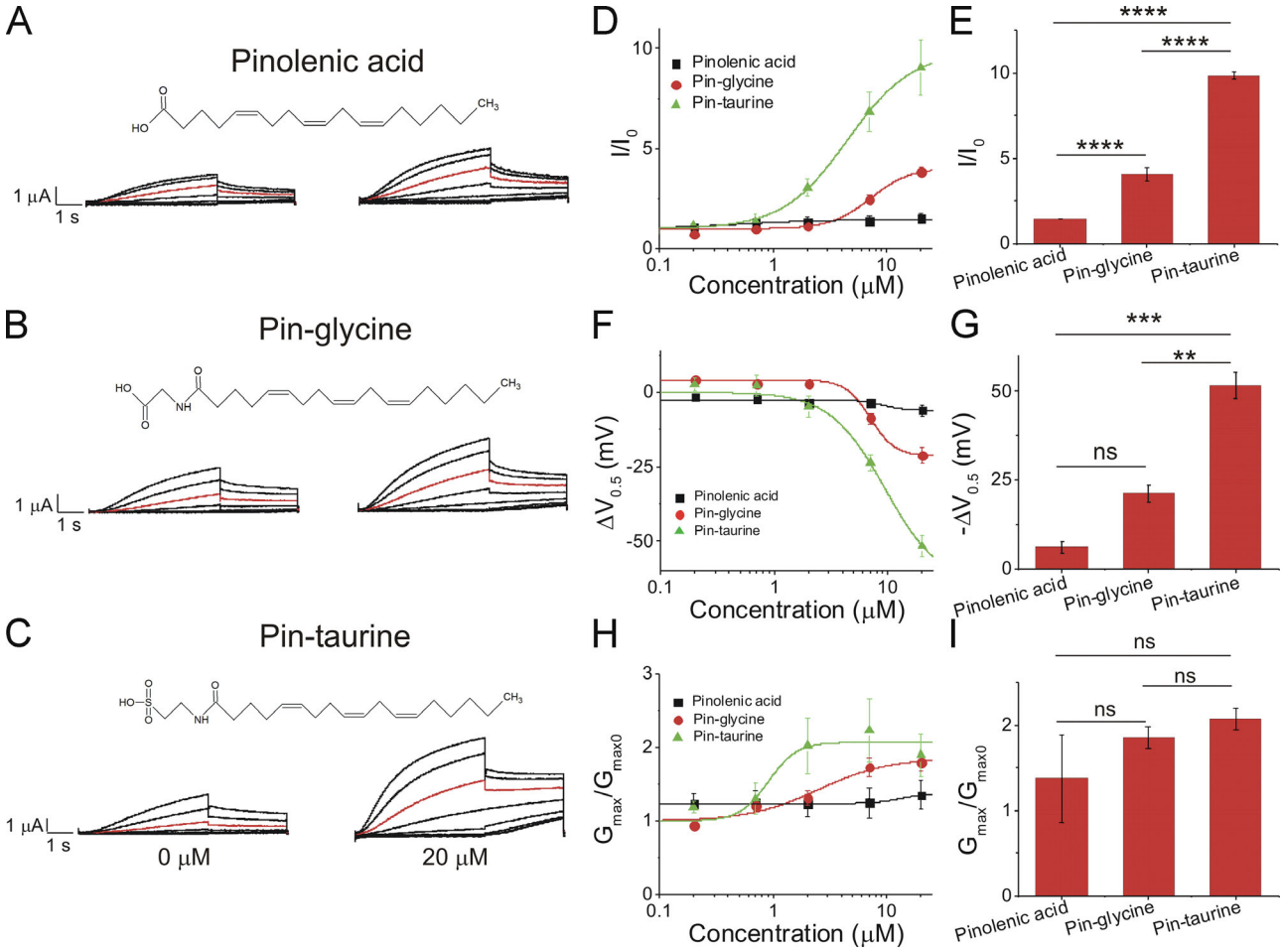

Figure 6. **Pin-taurine produces the most potent activation of the I_{Ks} channel compared with pin-glycine and pinolenic acid. (A–C)** Structure of and raw current traces measured in 0 μM (left) and 20 μM (right) (A) pinolenic acid, (B) pin-glycine, and (C) pin-taurine. Red trace shows currents at 20 mV for visualization of PUFA-induced effects on current. **(D)** Dose-dependent effects of pinolenic acid (n = 3), pin-glycine (n = 3), and pin-taurine (n = 4) on I_{Ks} current (I/I_0; mean ± SEM at maximal concentration). **(E)** Statistical differences on I/I_0 effects (I/I_0 fitted from the dose–response curve) measured by one-way ANOVA followed by Tukey's HSD post hoc analysis. **(F)** Dose-dependent effects of pinolenic acid, pin-glycine, and pin-taurine on I_{Ks} voltage dependence ($\Delta V_{0.5}$). **(G)** Statistical differences on $\Delta V_{0.5}$ effects ($\Delta V_{0.5}$ fitted from the dose–response curve) measured by one-way ANOVA followed by Tukey's HSD post hoc analysis. **(H)** Dose-dependent effects of pinolenic acid, pin-glycine, and pin-taurine on I_{Ks} G_{max}. **(I)** Statistical differences on G_{max} effects (G_{max} fitted from the dose–response curve) measured by one-way ANOVA followed by Tukey's HSD post hoc analysis. **, P < 0.01; ***, P < 0.001; ****, P < 0.0001. ns, not significant.

head group will be deprotonated and negatively charged at pH 7.5. PUFA analogues with a glycine head group produced similar max effects on I/I_0 (Fig. 7 A) and $\Delta V_{0.5}$ (Fig. 7 B), whereas G_{max} was more varied (Fig. 7 C). PUFA analogues with taurine head groups had an estimated pK_a of ∼2.6, suggesting that all of the PUFA molecules with a taurine head group will be deprotonated and negatively charged at pH 7.5. PUFA analogues with a taurine head group all produced much larger effects on $\Delta V_{0.5}$ than those with glycine head groups (Fig. 7 B), whereas the effects on G_{max} were all in a relatively similar range (Fig. 7 C). Lin-taurine and pin-taurine produced much larger effects on I/I_0 than those with glycine head groups, whereas DHA-taurine produced a similar effect on I/I_0 as those with glycine head groups (Fig. 7 A). In summary, the major difference between PUFAs with taurine and glycine head groups is in the effects on $\Delta V_{0.5}$. This difference is mainly due to the pK_a (i.e., the charge) of the PUFA head group, with little influence from the hydrophobic PUFA tail groups.

Hierarchical cluster analysis grouped PUFA analogues that have similar functional effects

We used hierarchical cluster analysis as an unbiased method to group PUFAs and PUFA analogues according to similarity of their effects on I/I_0, $\Delta V_{0.5}$, and G_{max} at 20 μM (Fig. 8 and Table 2). The hierarchical cluster analysis resulted in three distinct clusters of PUFAs and PUFA analogues. The first branch point results in the most distinct cluster (cluster 1) of PUFA analogues that include lin-taurine, lin-cysteic acid, pin-taurine, and DHA-taurine, which had the largest effects on the $V_{0.5}$. The second branch point divides clusters 2 and 3. Cluster 2 includes lin-aspartate, pin-glycine, DHA-glycine, and lin-glycine, which had intermediate effects on I/I_0 and G_{max}. Cluster 3 includes

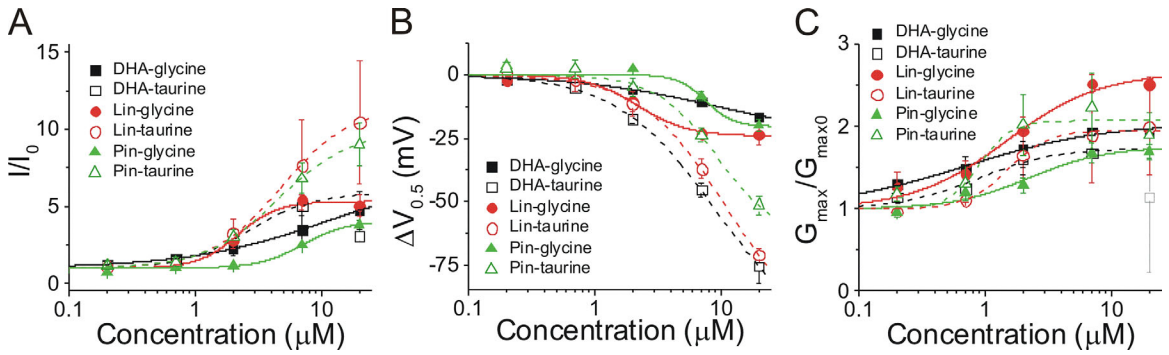

Figure 7. **Comparison of effects by glycine head groups and taurine head groups on I_{Ks} current (I/I_0), voltage dependence ($\Delta V_{0.5}$), and G_{max}. (A–C)** Dose-dependent effects of DHA-glycine (n = 4), lin-glycine (n = 4), pin-glycine (n = 3), DHA-taurine (n = 3), lin-taurine (n = 3), and pin-taurine (n = 4) on (A) I_{Ks} current (I/I_0), (B) I_{Ks} voltage dependence ($\Delta V_{0.5}$), and (C) I_{Ks} G_{max} (mean ± SEM at maximal concentration). Gray open square is for DHA-taurine at 20 μM (not included in fit).

linoleic acid, DHA, lin-AP3, and pinolenic acid, which had the smallest effects on I_{Ks} channel activation. The results of the hierarchical cluster analysis suggest that PUFA analogues with a glycine head group have the most consistent effects on increasing G_{max} and that PUFA analogues with a taurine head group are most consistent in left-shifting the voltage dependence of I_{Ks} channel activation.

Circulating concentrations of lin-glycine with albumin and other fatty acids promoted the activation of the cardiac I_{Ks} channel by left-shifting the voltage dependence of activation

In the body, PUFAs circulate in complex with serum albumin but interact with channel proteins in the free fatty acid form. In addition, PUFAs in the bloodstream are in circulation with other types of fatty acids, including MUFAs and SFAs. To emulate the effects of PUFAs under physiological conditions, we applied lin-glycine in combination with the MUFA oleic acid, the SFA stearic acid, and albumin (Tsukamoto and Sugawara, 2018; Abdelmagid et al., 2015). We applied 0.1 mM albumin/0.2 mM lin-glycine/0.2 mM oleic acid/0.2 mM stearic acid, which we refer to as albumin + fatty acids (Abdelmagid et al., 2015; Tsukamoto and Sugawara, 2018). Following the application of albumin + fatty acids, we saw an increase in I_{Ks} current (Fig. 9 A). In the current versus voltage relationship, we observed that the application of albumin + fatty acids increased G_{max} and caused a leftward shift in the voltage dependence of I_{Ks} activation (Fig. 9 B). Lin-glycine in combination with MUFAs, SFAs, and albumin produced a significant increase in I_{Ks} current (2.0 ± 0.1) compared with control (P = 0.003; Fig. 9 C). In addition, we observed a leftward shift in the voltage dependence of I_{Ks} activation (−11.4 ± 1.1 mV) compared with control (P = 0.0004) and a significant increase in the G_{max} of the I_{Ks} channel (1.15 ± 0.04; P = 0.007; Fig. 9, D and E). These data together suggest that there is still a substantial concentration of lin-glycine in the free fatty acid form that is available to promote the activation of the cardiac I_{Ks} channel by left-shifting the voltage dependence of activation and increasing G_{max}.

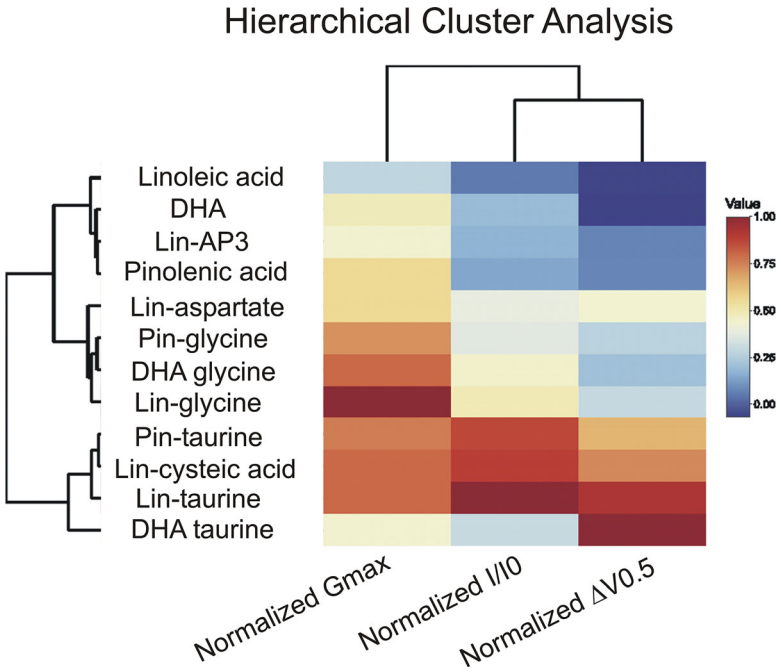

Figure 8. **Hierarchical cluster analysis and heat map demonstrate that taurine head groups are most similar in their voltage-shifting effects and glycine head groups are most similar in their effects on G_{max}.** The dendrogram displays groupings of PUFAs and PUFA analogues according to similarity of their effects. The heat map displays the magnitude of the effects, with warmer colors representing PUFAs and PUFA analogues that have larger relative effects (closer to 1.0) on I/I_0, G_{max}, and $\Delta V_{0.5}$ and cooler colors representing PUFAs and PUFA analogues with smaller relative effects (closer to 0.0).

Table 2. **Summary of effects of PUFA analogues on the cardiac I_{Ks} channel**

PUFA name	I/I_0	$\Delta V_{0.5}$ (mV)	G_{max}/G_{max0}	*n*
Linoleic acid	0.5 ± 0.04	4.7 ± 0.9	0.7 ± 0.04	5
Lin-glycine	5.3 ± 0.5	−26.4 ± 4.4	2.4 ± 0.2	4
Lin-taurine	10.4 ± 4.0	−73.1 ± 2.6	2.0 ± 0.6	3
Lin-glycine+1C	1.7 ± 0.2	−7.2 ± 2.5	1.3 ± 0.02	3
Lin-glycine+2C	1.9 ± 0.4	−8.7 ± 0.5	1.1 ± 0.2	3
Lin-cysteic acid	9.2 ± 0.4	−58.4 ± 2.8	2.0 ± 0.2	5
Lin-aspartate	4.0 ± 0.1	−34.5 ± 2.3	1.4 ± 0.1	4
Lin-AP3	1.8 ± 0.3	−5.7 ± 1.3	1.1 ± 0.1	3
DHA	2.0 ± 0.6	0.1 ± 1.4	1.7 ± 0.3	4
DHA-glycine	4.7 ± 1.3	−16.5 ± 1.3	2.0 ± 0.2	4
DHA-taurine	5.1 ± 0.7	−45.3 ± 2.9	1.7 ± 0.1	3
Pinolenic acid	1.5 ± 0.3	−6 ± 1.8	1.4 ± 0.2	3
Pin-glycine	3.8 ± 0.2	−21.1 ± 2.5	1.8 ± 0.1	3
Pin-taurine	9.0 ± 1.4	51.6 ± 3.5	1.9 ± 0.3	4

Summary of the effects of PUFAs on I_{Ks} I/I_0, $\Delta V_{0.5}$ (mV), and G_{max}/G_{max0} with the number of experiments (*n*). Data are represented as mean ± SEM at the maximum concentration used (effects of DHA-taurine are reported at 7 µM due to a decrease in current observed at 20 µM).

PUFA analogues rescued LQT1-associated loss-of-function mutation Kv7.1 V215M + KCNE1 by left-shifting voltage dependence of I_{Ks} activation

To evaluate the therapeutic potential of the PUFA analogues as potential treatments for LQTS, we expressed the I_{Ks} channel bearing a mutation that causes LQT1 (V215M). V215M (in which a valine residue is replaced with methionine) is a loss-of-function mutation located in the S3 segment of the Kv7.1 α subunit of the cardiac I_{Ks} channel (Eldstrom et al., 2010; Fig. 10 A). The V215M mutation causes a rightward shift in the voltage dependence of channel activation and alters the activation and deactivation kinetics compared with the wild-type channel

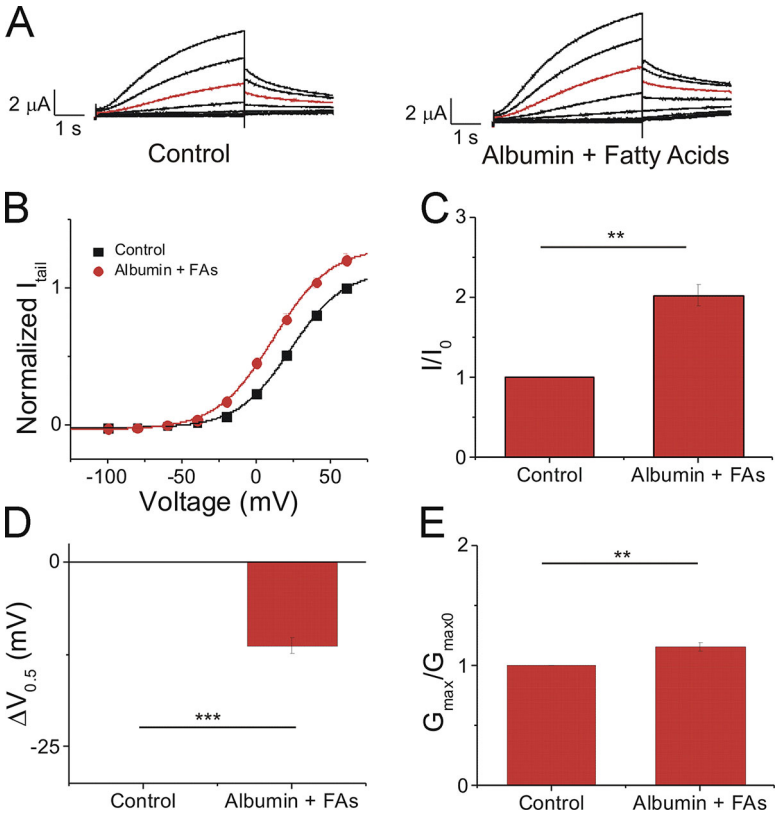

Figure 9. **Lin-glycine in combination with physiological concentrations of monounsaturated and saturated fatty acids and albumin promotes the activation of the I_{Ks} channel. (A)** Raw current traces measured in control ND96 (left) and in the presence of 0.1 mM albumin + 0.2 mM lin-glycine/0.2 mM oleic acid/0.2 mM stearic acid (Fatty Acids; right). Red trace shows currents at 20 mV for visualization of PUFA-induced effects on current. **(B)** Current-voltage relationship of cells in control ND96 (black squares) and in 0.1 mM albumin + 0.2 mM lin-glycine/0.2 mM oleic acid/0.2 mM stearic acid (fatty acids [FAs]; red circles; mean ± SEM; $n = 4$). **(C)** Statistical differences on I/I_0 effects (I/I_0 fitted from the dose–response curve) measured by one-way ANOVA followed by Tukey's HSD post hoc analysis. **(D)** Statistical differences on $\Delta V_{0.5}$ effects ($\Delta V_{0.5}$ fitted from the dose–response curve) measured by one-way ANOVA followed by Tukey's HSD post hoc analysis. **(E)** Statistical differences on G_{max} effects (G_{max} fitted from the dose–response curve) measured by one-way ANOVA followed by Tukey's HSD post hoc analysis. **, $P < 0.01$; ***, $P < 0.001$. ns, not significant.

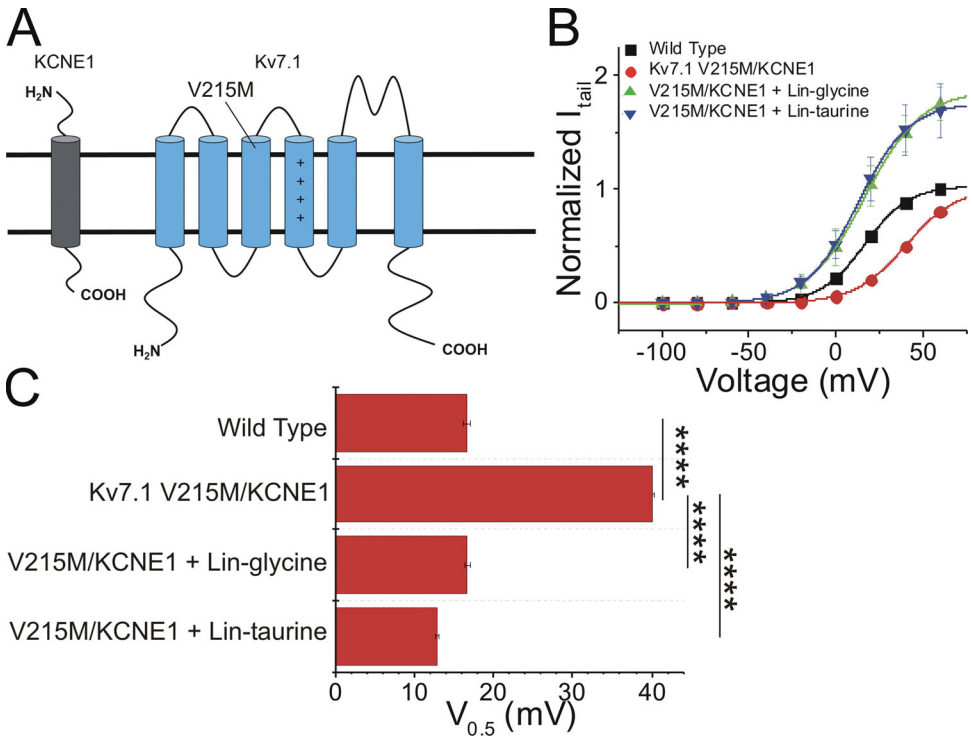

Figure 10. **PUFA analogues lin-glycine and lin-taurine rescue LQT1-associated loss-of-function mutation, V215M. (A)** Topology of Kv7.1 and KCNE1 with location of V215M indicated**. (B)** Current–voltage relationship of the wild-type I_{Ks} channel (black squares; mean ± SEM; *n* = 4), Kv7.1 V215M + KCNE1 (red circles; mean ± SEM; *n* = 3), Kv7.1 V215M + KCNE1 with lin-glycine (green triangles; mean ± SEM; *n* = 3), and Kv7.1 V215M + KCNE1 with lin-taurine (blue triangles; mean ± SEM; *n* = 3). **(C)** Statistical differences on the voltage dependence ($V_{0.5}$) effects ($V_{0.5}$ fitted using the Boltzmann equation) measured by one-way ANOVA followed by Tukey's HSD post hoc analysis. ****, P < 0.0001. Error bars represent SEM.

(Eldstrom et al., 2010). To determine the ability of PUFA analogues to restore I_{Ks} channel loss of function, we applied both lin-glycine and lin-taurine to the I_{Ks} channel bearing the V215M mutation. From the current versus voltage relationship, we found that the V215M mutation resulted in a significant rightward shift in the voltage dependence of I_{Ks} channel activation relative to the wild-type channel (V215M $V_{0.5}$ = 40.2 ± 0.2 mV; wild type $V_{0.5}$ = 16.6 ± 0.4 mV; and $\Delta V_{0.5}$ = +24.2 ± 2.3 mV; Fig. 10, B and C). However, the application of lin-glycine (at 10 µM) and lin-taurine (at 5 µM) both strongly left-shifted the voltage dependence of activation compared with the $V_{0.5}$ of activation of V215M mutant channels ($\Delta V_{0.5}$ = −23.8 ± 3.3 mV and −29.7 ± 0.8 mV, respectively), fully restoring the wild-type voltage dependence of the I_{Ks} channel (Fig. 10, B and C). These data demonstrating PUFA-induced effects on LQT1-causing mutations suggest that PUFA analogues are potent enough activators of the I_{Ks} channel that they are capable of restoring the normal voltage dependence of LQT1 mutation-bearing I_{Ks} channels.

Discussion

We have characterized several different head groups of PUFA analogues in order to determine the range of their effects of PUFA analogues on the current, voltage dependence, and G_{max} of the cardiac I_{Ks} channel. Our findings demonstrate that PUFA analogues with a glycine head group consistently produced moderate activation of the cardiac I_{Ks} channel. In addition, we demonstrated that PUFA analogues with a taurine or cysteic acid head group produced the most potent activation of the cardiac I_{Ks} channel. Lastly, we showed that increasing the number of potentially charged moieties did not necessarily improve PUFA-induced activation of the cardiac I_{Ks} channel. This is most likely due to the pK_a of the additional potentially charged moieties as well as potential steric hindrance of PUFAs with multiple potentially charged groups.

We previously presented evidence that the charged head group of PUFAs electrostatically interacts with the arginines in S4 or K326 in S6 of the I_{Ks} channel (Liin et al., 2018). We assume that the PUFAs and PUFA analogues tested here also interact by similar mechanisms with the I_{Ks} channel. As an example, we showed here that neutralization mutations of charges in S4 or S6 decrease the effects of lin-glycine on the voltage shift and G_{max} (Fig. S3), as if lin-glycine also interacts with the S4 arginines and K326 in the pore. Most of the variability in the effects of the different PUFA head groups on I_{Ks} channels can be explained by the predicted pK_a of the different head groups, which determines their protonation state in the membrane bound to the I_{Ks} channel. The experimentally determined pH dependence of the effect on I_{Ks} channels of a PUFA with a carboxyl head group was consistent with a pK_a of ∼8.5, suggesting that PUFAs with a simple carboxyl head group are protonated and neutral at pH 7.5. We therefore propose that PUFAs with a simple carboxyl head group are unable to participate in an electrostatic

interaction with S4 arginines or K326 in S6 the I_{Ks} channel. The experimental determined pK_a value of PUFA analogues with a glycine head group associated with the I_{Ks} channel is ∼7.6 (Börjesson and Elinder, 2011; Elinder and Liin, 2017; Liin et al., 2015). Therefore, half of the PUFA molecules with a glycine head group will be deprotonated and able to participate in an electrostatic interaction with S4 arginines or K326 in S6 (Liin et al., 2015). Our data comparing the effects of lin-glycine at pH 7.5 and pH 9.0 support the idea that half of the PUFA molecules with a glycine head group are able to have an electrostatic interaction with the S4 segment of I_{Ks} channels. Notably, the left-shift in the $V_{0.5}$ of lin-glycine at pH 9.0 (Fig. 3 H) was approximately doubled compared with the left-shift at pH 7.5 (Fig. 3 E), consistent with our estimate of a pK_a of ∼7.5–7.6 for PUFA analogues with glycine head groups (Table 1). At pH 9.0, all of the lin-glycine molecules will be deprotonated and able to participate in an electrostatic interaction with the S4 segment, leading to a larger left-shift in the voltage dependence of I_{Ks} channel activation.

Finally, the predicted pK_a for PUFA analogues with a taurine head group associated with I_{Ks} channels was ∼2.6, so all taurine head groups were able to participate in an electrostatic interaction with the S4 arginines or K326 in S6 even at pH 7.5. The predicted pK_as for taurine and glycine compounds are consistent with the approximate half size of the voltage-shifting effect of glycine compounds compared with taurine compounds. Why lin-glycine gives a larger increase in G_{max} than lin-taurine is not clear, but may be due to different access for lin-glycine than for lin-taurine to the PUFA binding site that promotes an increase in G_{max}. We estimated pK_{a1} and pK_{a2} values of lin-aspartate and lin-cysteic acid, as well as the pK_{a3} of lin-AP3, to compare them with estimated pK_a values of lin-glycine and lin-taurine (Table 1). In lin-aspartate, the pK_{a1} was ∼7.6, which is similar to the pK_a value of lin-glycine, suggesting that the first potentially charged group is likely to reside in its deprotonated form 50% of the time at pH 7.5. The pK_{a2} of lin-aspartate was ∼9.1, which means that the second potentially charged moiety would be protonated and uncharged at pH 7.5. Therefore, lin-aspartate has approximately the same functional charge on the hydrophilic head group as lin-glycine. Indeed, the overall effect of lin-aspartate on I/I_0 is not significantly different than the I/I_0 effect of lin-glycine. In lin-cysteic acid, the pK_{a1} was ∼2.4, which is very similar to the pK_a value of lin-taurine, meaning lin-cysteic acid should be at least as potent as lin-taurine. The pK_{a2} of lin-cysteic acid was ∼7.1, meaning that the second group is likely to reside in its deprotonated form >50% of the time at physiological pH. However, lin-cysteic acid did not have a larger effect than lin-taurine, suggesting that the second charge group was not interacting with the channel, or it is possible that nearby residues in the I_{Ks} channel protein modified the pK_{a2} so that this group remained protonated at pH 7.5. Lastly, in lin-AP3, the pK_{a1} and pK_{a2} were ∼5.0 and ∼7.7 while the pK_{a3} was ∼11.8, which suggests that the first site would be deprotonated and the second site would be deprotonated 50% of the time while the third group was protonated and uncharged at pH 7.5. However, lin-AP3 has little to no effect on I/I_0, $\Delta V_{0.5}$, or G_{max}, suggesting that lin-AP3 does not effectively interact with the voltage sensor/pore or that it is not effectively deprotonated/negatively charged. We observed small effects of lin-AP3 when applied at pH 9.0 (in an attempt to help unmask potentially charged groups; Fig. S4), suggesting that there may be steric hindrance preventing the bulky AP3 head group from interacting favorably with the I_{Ks} channel.

Similar to our findings on the importance of the pK_a of the PUFAs for shifting the voltage dependence of I_{Ks} channels, Ottosson et al. (2015) found that lowering the pK_a of resin acid molecules resulted in greater left shift in the voltage dependence of the Shaker potassium channel. This further shows the importance of a deprotonated and charged compound for a strong activating effect on voltage-gated K^+ channels by the lipoelectric mechanism. In addition, they noted that with some substitutions wherein a bulky group was added to the scaffold, the efficacy of these resin acid compounds was reduced (Ottosson et al., 2015). They suggested that adding a bulky group may impede the ability of the small molecule to interact with the voltage sensor of the Shaker K^+ channel (Ottosson et al., 2015). This is similar to our data using the more bulky PUFA analogue lin-AP3.

The pH dependence of PUFA head group ionization was also shown in the Slo1 BK channel by Tian et al. (2016). They found that DHA produces potent activation of Slo1 BK channels and that this effect can be reduced when the pH is decreased, leading to protonation of the PUFA head group, and that the effect can be potentiated when the pH is increased, leading to deprotonation of the PUFA head group (Tian et al., 2016). Similar to our results, Tian et al. (2016) found that the addition of a phosphate head group leads to an attenuated effect on BK channel activation compared with DHA and DHA-glycine, which is similar to the effects we saw when applying lin-AP3.

In addition to the charge of the PUFA head group, the degree of unsaturation in the PUFA tail also plays an important role in PUFA-induced activation of the I_{Ks} channel. We and others have found that the PUFA-induced activation of I_{Ks} channels and Shaker K channels requires that the PUFA tail structure has at least two double bonds in cis-configuration in the tail (Liin et al., 2015, 2016; Börjesson et al., 2008). We recently conducted a systematic analysis of the PUFA tail (Bohannon et al., 2019) and found that neither the length of the carbon tail nor the number of double bonds in the tail correlated significantly with effects on or apparent binding affinity for the cardiac I_{Ks} channel. However, the position of the double bonds in the tail was strongly correlated with stronger activation of and better apparent affinity for the cardiac I_{Ks} channel (Bohannon et al., 2019).

Lipophilic compounds have the ability to form micelles. The concentration at which micelle formation takes place is called the critical micellar concentration. If the critical micellar concentration for our compounds was reached, micelle formation had the potential to interfere with the efficacy of the PUFAs and PUFA analogues being applied. However, the critical micellar concentration that is estimated for the majority of PUFAs and other unsaturated fatty acids is between 60 and 150 µM (Serth et al., 1991; Richieri et al., 1992; Mukerjee and Mysels, 1971). The experiments reported here were done at concentrations

between 0.2 and 20 µM, which is well under the expected critical micellar concentration reported for unsaturated fatty acids. For this reason, we expect that the PUFAs applied in our preparation remained in the free fatty acid form, meaning that it is unlikely that any lack of effect from a PUFA could be attributed to the formation of micelles.

A range of effective compounds for activating the cardiac I_{Ks} channel is useful in the design of personalized therapeutics for LQT1. Patients with different LQT1 mutations have I_{Ks} channels with different degrees of channel malfunction (e.g., different-sized voltage shifts in their voltage dependence of activation) and present symptoms of varying severity. For this reason, individual LQT1 patients will not benefit from a one-size-fits-all treatment, producing a need for more personalized treatments. The findings presented here suggest that patients with more severe loss-of-function mutations of the cardiac I_{Ks} channel would most likely benefit from PUFA analogues with a taurine head group. In particular, PUFA analogues with a taurine or cysteic acid head group would be the most effective to rescue loss-of-function mutations in the I_{Ks} channel that lead to large shifts of the voltage dependence of I_{Ks} activation because these head groups produce the most robust effects on the $V_{0.5}$. Patients with a milder LQT1 phenotype, however, may benefit more from treatment with a glycine PUFA analogue that has more moderate effects on I_{Ks} channel activation, and especially loss-of-function mutations that alter the G_{max} of the I_{Ks} channel. Effective PUFA analogues can thus be selected for specific patients according to the severity of LQT1 pathology.

Acknowledgments

Sharona E. Gordon served as editor.

We thank Thea Wennman, Amanda Dahl, Frida Marshagen, Fiola Beqiri, Levi Lindroos, and Sankhero Gewarges for their contributions to experiments during their time as visiting scholars at the University of Miami. We thank Dr. Peter Konradsson at Linköping University for valuable discussions regarding synthesis strategies.

This work was supported by National Institutes of Health R01-HL131461 (to H.P. Larsson) and by the Swedish Society for Medical Research and the Swedish Research Council (2017-02040 to S.I. Liin).

A patent application (62/032,739) has been submitted by the University of Miami with S.I. Liin and H.P. Larsson as inventors. The other authors declare no competing financial interests.

Author Contributions: B.M. Bohannon, acquisition of data, analysis and interpretation of data, and drafting or revising the article; H.P. Larsson, conception and design, analysis and interpretation of data, and drafting or revising the article; S.I. Liin, conception and design, acquisition of data, analysis and interpretation of data, and drafting or revising the article; M.E. Perez, acquisition of data; X. Wu, contributing new compounds and acquisition of data.

Submitted: 8 May 2019
Revised: 5 September 2019
Accepted: 27 November 2019

References

Abdelmagid, S.A., S.E. Clarke, D.E. Nielsen, A. Badawi, A. El-Sohemy, D.M. Mutch, D.W.L. Ma, and P.L.O.S.O.N.E. Staff. PLOS ONE Staff. 2015. Correction: Comprehensive profiling of plasma fatty acid concentrations in young healthy Canadian adults. *PLoS One.* 10:e0128167. https://doi.org/10.1371/journal.pone.0116195

Alders, M., and I. Christiaans. 2003. Long QT syndrome. *In* GeneReviews. M.P. Adam, H.H. Ardinger, R.A. Pagon, S.E. Wallace, L.J.H. Bean, K. Stephens, and A. Amemiya, editors. [Internet]. University of Washington, Seattle. 1993–2019.

Amin, A.S., J.R. Giudicessi, A.J. Tijsen, A.M. Spanjaart, Y.J. Reckman, C.A. Klemens, M.W. Tanck, J.D. Kapplinger, N. Hofman, M.F. Sinner, et al. 2012. Variants in the 3′ untranslated region of the KCNQ1-encoded Kv7.1 potassium channel modify disease severity in patients with type 1 long QT syndrome in an allele-specific manner. *Eur. Heart J.* 33: 714–723. https://doi.org/10.1093/eurheartj/ehr473

Barhanin, J., F. Lesage, E. Guillemare, M. Fink, M. Lazdunski, and G. Romey. 1996. $K_{(V)}$LQT1 and lsK (minK) proteins associate to form the $I_{(Ks)}$ cardiac potassium current. *Nature.* 384:78–80. https://doi.org/10.1038/384078a0

Barro-Soria, R., S. Rebolledo, S.I. Liin, M.E. Perez, K.J. Sampson, R.S. Kass, and H.P. Larsson. 2014. KCNE1 divides the voltage sensor movement in KCNQ1/KCNE1 channels into two steps. *Nat. Commun.* 5:3750–3761. https://doi.org/10.1038/ncomms4750

Bohannon, B.M., M.E. Perez, S.I. Liin, and H.P. Larsson. 2019. ω-6 and ω-9 polyunsaturated fatty acids with double bonds near the carboxyl head have the highest affinity and largest effects on the cardiac I_{Ks} potassium channel. *Acta Physiol. (Oxf.).* 225:e13186. https://doi.org/10.1111/apha.13186

Bohnen, M.S., G. Peng, S.H. Robey, C. Terrenoire, V. Iyer, K.J. Sampson, and R.S. Kass. 2017. Molecular Pathophysiology of Congenital Long QT Syndrome. *Physiol. Rev.* 97:89–134. https://doi.org/10.1152/physrev.00008.2016

Börjesson, S.I., and F. Elinder. 2011. An electrostatic potassium channel opener targeting the final voltage sensor transition. *J. Gen. Physiol.* 137: 563–577. https://doi.org/10.1085/jgp.201110599

Börjesson, S.I., S. Hammarström, and F. Elinder. 2008. Lipoelectric modification of ion channel voltage gating by polyunsaturated fatty acids. *Biophys. J.* 95:2242–2253. https://doi.org/10.1529/biophysj.108.130757

Cho, Y. 2016. Management of Patients with Long QT Syndrome. *Korean Circ. J.* 46:747–752. https://doi.org/10.4070/kcj.2016.46.6.747

Chockalingam, P., L. Crotti, G. Girardengo, J.N. Johnson, K.M. Harris, J.F. van der Heijden, R.N.W. Hauer, B.M. Beckmann, C. Spazzolini, R. Rordorf, et al. 2012. Not all beta-blockers are equal in the management of long QT syndrome types 1 and 2: higher recurrence of events under metoprolol. *J. Am. Coll. Cardiol.* 60:2092–2099. https://doi.org/10.1016/j.jacc.2012.07.046

Chouabe, C., N. Neyroud, P. Richard, I. Denjoy, B. Hainque, G. Romey, M.D. Drici, P. Guicheney, and J. Barhanin. 2000. Novel mutations in KvLQT1 that affect Iks activation through interactions with Isk. *Cardiovasc. Res.* 45:971–980. https://doi.org/10.1016/S0008-6363(99)00411-3

Crotti, L., C. Spazzolini, P.J. Schwartz, W. Shimizu, I. Denjoy, E. Schulze-Bahr, E.V. Zaklyazminskaya, H. Swan, M.J. Ackerman, A.J. Moss, et al. 2007. The common long-QT syndrome mutation KCNQ1/A341V causes unusually severe clinical manifestations in patients with different ethnic backgrounds: toward a mutation-specific risk stratification. *Circulation.* 116:2366–2375. https://doi.org/10.1161/CIRCULATIONAHA.107.726950

Drum, B.M.L., R.E. Dixon, C. Yuan, E.P. Cheng, and L.F. Santana. 2014. Cellular mechanisms of ventricular arrhythmias in a mouse model of Timothy syndrome (long QT syndrome 8). *J. Mol. Cell. Cardiol.* 66:63–71. https://doi.org/10.1016/j.yjmcc.2013.10.021

Eldstrom, J., H. Xu, D. Werry, C. Kang, M.E. Loewen, A. Degenhardt, S. Sanatani, G.F. Tibbits, C. Sanders, and D. Fedida. 2010. Mechanistic basis for LQT1 caused by S3 mutations in the KCNQ1 subunit of I_{Ks}. *J. Gen. Physiol.* 135:433–448. https://doi.org/10.1085/jgp.200910351

Elinder, F., and S.I. Liin. 2017. Actions and mechanisms of polyunsaturated fatty acids on voltage-gated ion channels. *Front. Physiol.* 8:43. https://doi.org/10.3389/fphys.2017.00043

Harmer, S.C., A.J. Wilson, R. Aldridge, and A. Tinker. 2010. Mechanisms of disease pathogenesis in long QT syndrome type 5. *Am. J. Physiol. Cell Physiol.* 298:C263–C273. https://doi.org/10.1152/ajpcell.00308.2009

Larsson, J.E., H.P. Larsson, and S.I. Liin. 2018. KCNE1 tunes the sensitivity of $K_V7.1$ to polyunsaturated fatty acids by moving turret residues close to the binding site. *eLife.* 7:e37257. https://doi.org/10.7554/eLife.37257

Liin, S.I., M. Silverå Ejneby, R. Barro-Soria, M.A. Skarsfeldt, J.E. Larsson, F. Starck Härlin, T. Parkkari, B.H. Bentzen, N. Schmitt, H.P. Larsson, and F. Elinder. 2015. Polyunsaturated fatty acid analogs act antiarrhythmically on the cardiac I_{Ks} channel. *Proc. Natl. Acad. Sci. USA.* 112: 5714–5719. https://doi.org/10.1073/pnas.1503488112

Liin, S.I., J.E. Larsson, R. Barro-Soria, B.H. Bentzen, and H.P. Larsson. 2016. Fatty acid analogue N-arachidonoyl taurine restores function of I_{Ks} channels with diverse long QT mutations. *eLife.* 5:e20272. https://doi.org/10.7554/eLife.20272

Liin, S.I., S. Yazdi, R. Ramentol, R. Barro-Soria, and H.P. Larsson. 2018. Mechanisms Underlying the Dual Effect of Polyunsaturated Fatty Acid Analogs on Kv7.1. *Cell Reports.* 24:2908–2918. https://doi.org/10.1016/j.celrep.2018.08.031

Mukerjee, P., and K.J. Mysels. 1971. National Standards Reference Data Service. National Bureau of Standards, Washington, D.C.

Osteen, J.D., C. Gonzalez, K.J. Sampson, V. Iyer, S. Rebolledo, H.P. Larsson, and R.S. Kass. 2010. KCNE1 alters the voltage sensor movements necessary to open the KCNQ1 channel gate. *Proc. Natl. Acad. Sci. USA.* 107: 22710–22715. https://doi.org/10.1073/pnas.1016300108

Ottosson, N.E., X. Wu, A. Nolting, U. Karlsson, P.E. Lund, K. Ruda, S. Svensson, P. Konradsson, and F. Elinder. 2015. Resin-acid derivatives as potent electrostatic openers of voltage-gated K channels and suppressors of neuronal excitability. *Sci. Rep.* 5:13278. https://doi.org/10.1038/srep13278

Peroz, D., N. Rodriguez, F. Choveau, I. Baró, J. Mérot, and G. Loussouarn. 2008. Kv7.1 (KCNQ1) properties and channelopathies. *J. Physiol.* 586: 1785–1789. https://doi.org/10.1113/jphysiol.2007.148254

Richieri, G.V., R.T. Ogata, and A.M. Kleinfeld. 1992. A fluorescently labeled intestinal fatty acid binding protein. Interactions with fatty acids and its use in monitoring free fatty acids. *J. Biol. Chem.* 267: 23495–23501.

Rivolta, I., C.E. Clancy, M. Tateyama, H. Liu, S.G. Priori, and R.S. Kass. 2002. A novel SCN5A mutation associated with long QT-3: altered inactivation kinetics and channel dysfunction. *Physiol. Genomics.* 10:191–197. https://doi.org/10.1152/physiolgenomics.00039.2002

Salata, J.J., N.K. Jurkiewicz, B. Jow, K. Folander, P.J. Guinosso Jr., B. Raynor, R. Swanson, and B. Fermini. 1996. I_K of rabbit ventricle is composed of two currents: evidence for $I_{Ks.}$ *Am. J. Physiol.* 271:H2477–H2489.

Sanguinetti, M.C., M.E. Curran, A. Zou, J. Shen, P.S. Spector, D.L. Atkinson, and M.T. Keating. 1996. Coassembly of K(V)LQT1 and minK (IsK) proteins to form cardiac $I_{(Ks)}$ potassium channel. *Nature.* 384:80–83. https://doi.org/10.1038/384080a0

Schwartz, P.J., L. Crotti, and R. Insolia. 2012. Long-QT syndrome: from genetics to management. *Circ Arrhythm Electrophysiol.* 5:868–877. https://doi.org/10.1161/CIRCEP.111.962019

Schwartz, P.J., M.J. Ackerman, and A.A.M. Wilde. 2017. Channelopathies as Causes of Sudden Cardiac Death. *Card. Electrophysiol. Clin.* 9:537–549. https://doi.org/10.1016/j.ccep.2017.07.005

Serth, J., A. Lautwein, M. Frech, A. Wittinghofer, and A. Pingoud. 1991. The inhibition of the GTPase activating protein-Ha-ras interaction by acidic lipids is due to physical association of the C-terminal domain of the GTPase activating protein with micellar structures. *EMBO J.* 10: 1325–1330. https://doi.org/10.1002/j.1460-2075.1991.tb07651.x

Smith, J.A., C.G. Vanoye, A.L. George Jr., J. Meiler, and C.R. Sanders. 2007. Structural models for the KCNQ1 voltage-gated potassium channel. *Biochemistry.* 46:14141–14152. https://doi.org/10.1021/bi701597s

Tian, Y., M. Aursnes, T.V. Hansen, J.E. Tungen, J.D. Galpin, L. Leisle, C.A. Ahern, R. Xu, S.H. Heinemann, and T. Hoshi. 2016. Atomic determinants of BK channel activation by polyunsaturated fatty acids. *Proc. Natl. Acad. Sci. USA.* 113:13905–13910. https://doi.org/10.1073/pnas.1615562113

Tsukamoto, I., and S. Sugawara. 2018. Low levels of linoleic acid and α-linolenic acid and high levels of arachidonic acid in plasma phospholipids are associated with hypertension. *Biomed. Rep.* 8:69–76.

Waddell-Smith, K.E., and J.R. Skinner. members of the CSANZ Genetics Council Writing Group. 2016. Update on the Diagnosis and Management of Familial Long QT Syndrome. *Heart Lung Circ.* 25:769–776. https://doi.org/10.1016/j.hlc.2016.01.020

Wu, J., W.G. Ding, and M. Horie. 2016. Molecular pathogenesis of long QT syndrome type 1. *J. Arrhythm.* 32:381–388. https://doi.org/10.1016/j.joa.2015.12.006

JGP

Supplemental material

Bohannon et al., https://doi.org/10.1085/jgp.201912396

Compound synthesis

Materials and methods

Most of the reagents are from Sigma-Aldrich except *O*-(benzotriazol-1-yl)-*N*,*N*,*N*′,*N*′-tetramethyluronium tetrafluoroborate (TBTU; Fluka) and pinolenic acid (Cayman). Preparative liquid chromatography (LC) was run using a Waters system with an XSELECT Phenyl-Hexyl column (250 × 19 mm, 5 µm) under neutral conditions with gradient CH_3CN/water as eluent (A, water phase: 95:5 water/CH_3CN, 10 mM NH_4OAc; B, organic phase: 90:10 CH_3CN/water, 10 mM NH_4OAc) at a flow rate of 25 ml/min in 12 min using an electrospray light scatter detector. The NMR spectra were recorded on a Varian Advance 300 MHz with solvent indicated. Chemical shift of NMR is reported in parts per million on the δ scale and referenced to the solvent peak ($CDCl_3$: δ_H = 7.26 ppm, δ_C = 77.16 ppm).

General procedure for the compound synthesis

To the unsaturated aliphatic acid (1.0 equivalent [equiv]) and triethylamine (2.2 equiv) in acetonitrile (10 ml) or *N*,*N*-dimethylformamide (DMF), 1.05 equiv TBTU was added. The reaction mixture was stirred at room temperature (rt) for about 30 min. Amino acid or its analogue (1.20 equiv) was added at rt and stirred overnight/s. The reaction was monitored using TLC or liquid chromatography–mass spectrometry. The solution was filtered after or without workup and purified using preparative LC or normal silica gel chromatography. The desired fractions were combined and concentrated to remove the solvent to give the desired product. For products containing a strong acidic group of -SO_3H or -PO_3H_2, the fractions were combined and concentrated followed by the addition of water. The resulting solution was adjusted to a pH of about 2 using 2 M HCl aqueous solution and extracted with ethyl acetate. The organic layers were combined and concentrated to give the desired product.

DHA-taurine: Following the general procedure with DHA (17.0 mg, 0.052 mmol), TBTU (19.9 mg, 0.062 mmol), diisopropylethylamine (26.9 mg, 0.208 mmol), and taurine (7.8 mg, 0.062 mmol) as starting materials and DMF (1 ml) as solvent, the reaction mixture was stirred overnight at rt, filtered, and purified using preparative LC (B:A: from 40:60 to 100:0). The fractions were combined, diluted with water (3 ml), and acidified with 2M HCl to about pH 2–3, then extracted with ethyl acetate 5 ml × 3. The organic layer was concentrated to give the product (21.7 mg, 91%). ^{1}H NMR ($CDCl_3$, 300 MHz): δ 5.47-5.21 (multiplet [m], 12H), 3.86-3.58 (m, 2H), 3.27-3.05 (m, 2H), 2.89-2.69 (m, 12H), 2.61-2.29 (m, 4H), 2.13-1.97 (m, 2H), and 0.96 (t, *J* = 7.5 Hz, 3H). ^{13}C NMR ($CDCl_3$, 75 MHz): δ 176.9, 132.2, 130.5, 128.8, 128.54, 128.50, 128.2, 128.0, 127.9, 127.2, 126.9, 49.6, 37.0, 34.8, 25.8, 25.7, 23.6, 20.7, and 14.4. mass spectrum with electrospray ionization: MS (ESI$^-$): calculated (calcd) for $C_{25}H_{36}NO_4$: 434.24 $(M-H)^-$; found 434.58.

Linoleoyl glycine: To the mixture of linoleic acid (334.0 mg, 1.19 mmol) and triethylamine (265.2 mg, 2.62 mmol) in acetonitrile (CH_3CN, 20 ml), TBTU was added (401.5 mg, 1.25 mmol). The mixture was stirred at rt for about 1 h. Glycine (107.3 mg, 1.43 mmol) was added to the mixture and stirred over two nights. The mixture was concentrated, redissolved in 25 ml dichloromethane, and washed with water (15 ml). The organic layer was concentrated and purified using ethyl acetate/n-heptane/HCOOH (35:65:0.3 to 60:40:0.3) with silica gel chromatography to give the title product as a white solid (173.0 mg, 43%). ^{1}H NMR ($CDCl_3$, 300 MHz): δ 10.48 (broad singlet [br s], 1H), 6.39 (triplet [t], *J* = 4.8 Hz, 1H, NH), 5.40-5.26 (m, 4H), 4.05 (d, *J* = 4.8 Hz, 2H), 2.76 (t, *J* = 6.0 Hz, 2H), 2.27 (t, *J* = 7.8 Hz, 2H), 2.31-2.20 (m, 2H), 1.68-1.68 (m, 2H), 1.40-1.20 (m, 14H), and 0.88 (t, *J* = 6.9 Hz, 3H). ^{13}C NMR ($CDCl_3$, 75 MHz): δ 174.9, 172.9, 130.4, 130.1, 128.2, 128.0, 41.6, 36.4, 31.6, 29.7, 29.5, 29.4, 29.3, 29.2, 27.3, 25.8, 25.7, 22.7, and 14.2. MS (ESI$^-$): calcd for $C_{20}H_{34}NO_3$: 336.25 $[M-H]^-$; found: 336.50.

Linoleoyl taurine: Following the general procedure, DHA (140.2 mg, 0.500 mmol), TBTU (192.6 mg, 0.600 mmol), diisopropylethylamine (258.5 mg, 2.000 mmol), and taurine (75.1 mg, 0.600 mmol) were used as starting materials, and acetonitrile (20 ml) as solvent. The product lost during extensive purifications using silica gel and preparative LC with a UV detector. Eventually, after acidifying, extraction, and concentration, the title compound was achieved (4 mg, 4%). The purification could have been better if the electrospray light scatter detector was used as the detector. ^{1}H NMR ($CDCl_3$, 300 MHz): δ 5.42-5.21 (m, 4H), 3.95-3.60 (m, 2H), 3.30-3.15 (m, 2H), 2.75 (t, *J* = 6.3 Hz, 2H), 2.62-2.40 (m, 2H), 2.10-1.90 (m, 2H), 1.75-1.55 (m, 2H), 1.40-1.19 (m, 16H), and 0.89 (t, *J* = 6.9 Hz, 3H). ^{13}C NMR ($CDCl_3$, 75 MHz): δ 178.3, 130.4, 130.0, 128.3, 128.0, 49.2, 37.3, 34.7, 31.6, 29.9, 29.5, 29.4, 29.3, 29.2, 27.4, 27.3, 26.0, 25.8, 22.7, and 14.2. MS (ESI$^-$): calcd for $C_{20}H_{36}NO_4S$: 386.24 $[M-H]^-$; found: 386.42.

Linoleoyl glycine+1C: The title compound was synthesized using the general method with linoleic acid (111.0 mg, 0.396 mmol), TBTU (133.6 mg, 0.416 mmol), triethylamine (88.2 mg, 0.871 mmol), and β-alanine (42.3 mg, 0.475 mmol) as starting materials and acetonitrile (10 ml) as solvent. The reaction mixture was concentrated, redissolved in 25 ml dichloromethane, and washed with 15 ml of water. The organic layer was concentrated and purified using silica gel chromatography twice, firstly with ethyl acetate/

n-heptane/HCOOH (35:65:0.3 to 100:0:0.3) and secondly with methanol/dichloromethane/HCOOH (4:96:0.3 to 6:94:0.3) to give the title compound (11.7 mg, 8%) as a white solid. ^{1}H NMR ($CDCl_3$, 300 MHz): δ 6.15 (br s, 1H), 5.43-5.28 (m, 4H), 3.58-3.48 (m, 2H), 2.76 (t, *J* = 6.0 Hz, 2H), 2.59 (t, *J* = 6.0 Hz, 2H), 2.17 (t, *J* = 6.0 Hz, 2H), 2.10-1.99 (m, 4H), 1.65-1.55, (m, 2H), 1.40-1.20 (m, 14H), and 0.89 (t, *J* = 6.0 Hz, 3H). ^{13}C NMR ($CDCl_3$, 75 MHz): δ 176.7, 174.0, 130.4, 130.2, 128.2, 128.1, 36.9, 34.9, 34.0, 31.7, 29.8, 29.5, 29.4, 29.36, 29.3, 27.4, 25.8, 25.78, 22.7, and 14.2. MS (ESI$^-$): calcd for $C_{21}H_{36}NO_3$: 350.27 [M-H]$^-$; found: 350.56.

Linoleoyl glycine+2C: The title compound was synthesized using the same method for the synthesis of linoleoyl glycine+1C with linoleic acid (111.0 mg, 0.396 mmol), TBTU (133.6 mg, 0.416 mmol), triethylamine (88.2 mg, 0.871 mmol), and β-alanine (49.0 mg, 0.475 mmol) as starting materials and acetonitrile (10 ml) as solvent. The reaction mixture was concentrated, redissolved in 25 ml of dichloromethane, and washed with 15 ml of water. The organic layer was concentrated and purified using silica gel chromatography twice, firstly with ethyl acetate/n-heptane/HCOOH (35:65:0.3 to 60:40:0.3) and secondly with methanol/dichloromethane/HCOOH (3:97:0.3 to 5:95:0.3) to give the title compound (25.9 mg, 18%) as a white solid. ^{1}H NMR ($CDCl_3$, 300 MHz): δ 5.86 (br s, 1H), 5.45-5.25 (m, 4H), 3.39-3.35 (m, 2H), 2.76 (t, *J* = 6.0 Hz, 2H), 2.40 (t, *J* = 6.0 Hz, 2H), 2.18 (t, *J* = 7.5 Hz, 2H), 1.89-1.78 (m, 2H), 1.65-1.55 (m, 2H), 1.35-1.25 (m, 14H), and 0.88 (t, *J* = 6.0 Hz, 3H). ^{13}C NMR ($CDCl_3$, 75 MHz): δ 177.2, 174.2, 130.4, 130.2, 128.2, 128.1, 39.0, 38.8, 36.9, 31.7, 31.6, 29.8, 29.5, 29.4, 29.3, 27.4, 25.9, 25.8, 25.0, 22.7, and 14.2. MS (ESI$^-$): calcd for $C_{22}H_{38}NO_3$: 364.29 [M-H]$^-$; found: 364.52.

Linoleoyl aspartate: The title compound was synthesized in two steps by first coupling with L-aspartate acid methyl ester, then hydrolysis using lithium hydroxide (LiOH) aqueous solution.

Step 1: To the mixture of linoleic acid (111.0 mg, 0.396 mmol) and diisopropylethylamine (112.6 mg, 0.871 mmol) in acetonitrile (10 ml), TBTU (133.6 mg, 0.416 mmol) at rt was added. The mixture was stirred overnight, concentrated, and purified on silica gel with ethyl acetate/n-heptane/HCOOH (25:75:0.5 to 35:65:0.5) to give the amide coupling product (163.0 mg, 97%). ^{1}H NMR ($CDCl_3$, 300MHz): δ 6.46 (d, *J* = 7.8 Hz, 1H), 5.41-5.25 (m, 4H), 4.85 (m, 1H), 3.74 (s, 3H), 3.67 (s, 3H), 3.00 (dd, *J* = 17.1, 4.2 Hz, 1H), 2.83 (dd, *J* = 17.1, 4.2 Hz, 1H), 2.75 (t, *J* = 6.0 Hz, 2H), 2.20 (t, *J* = 7.4 Hz, 2H), 2.08-1.94 (m, 4H), 1.68-1.54 (m, 2H), 1.40-1.20 (m, 14H), and 0.87 (t, *J* = 6.9 Hz, 3H). ^{13}C NMR ($CDCl_3$, 75 MHz): δ 173.0, 171.7, 171.4, 130.3, 130.1, 128.1, 128.0, 52.8, 52.1, 48.4, 36.6, 36.2, 31.6, 29.7, 29.4, 29.3, 29.2, 27.3, 25.7, 25.6, 22.7, and 14.2.

Step 2: The mixture of the resulting amide coupling product (76.1 mg, 0.180 mmol), LiOH⊠H_2O (56.4 mg, 1.334 mmol), and tetrahydrofuran/water (6 ml/2 ml) was stirred overnight. The reaction mixture was adjusted with 2M HCl aqueous solution to pH at about 4–5, preabsorbed on silica gel, and purified using silica gel chromatography with ethyl acetate/n-heptane/HCOOH (30:70:0.5 to 70:30:0.5) to give the title compound (67.5 mg, 95%). ^{1}H NMR ($CDCl_3$, 300MHz): δ 107 (br s, 2H), 7.02 (d, *J* = 7.5 Hz, 1H, NH), 5.40-5.29 (m, 4H), 4.92-4.86 (m, 1H), 3.12-2.82 (m, 2H), 2.76 (t, *J* = 5.8 Hz, 2H), 2.28-2.20 (m, 2H), 2.10-1.95 (m, 4H), 1.68-1.50 (m, 2H), 1.48-1.25 (m, 14H), and 0.88 (t, *J* = 6.6 Hz, 3H). ^{13}C NMR ($CDCl_3$, 75 MHz): δ 175.6, 174.9, 174.8, 130.4, 130.1, 128.2, 128.0, 48.6, 36.3, 36.2, 31.6, 29.8, 29.5, 29.4, 29.3, 27.3, 25.8, 25.6, 22.7, and 14.2. MS (ESI$^-$): calcd for $C_{22}H_{36}NO_5$: 394.26 [M-H]$^-$; found: 394.52.

Linoleoyl cysteic acid: The title compound was synthesized using the general method with linoleic acid (111.0 mg, 0.396 mmol), TBTU (133.6 mg, 0.416 mmol), triethylamine (88.2 mg, 0.871 mmol), and L-cysteic acid (80.4 mg, 0.475 mmol) as starting materials and acetonitrile as solvent (10 ml). The reaction mixture was stirred overnight at rt, concentrated, and purified using preparative LC (eluent: B:A: from 15:85 to 100:0). The fractions were combined, diluted with water (10 ml), and acidified with 2M HCl to about pH 2–3, then extracted with ethyl acetate 25 ml × 3. The organic layers were combined and concentrated to give the title product (133.0 mg, 78%). ^{1}H NMR ($CDCl_3$, 300 MHz): δ 11.9 (br s, 2H), 5.40-5.25 (m, 4H), 4.99 (br S, 1H), 3.58 (m, 2H), 2.78-2.40 (m, 4H), 2.20-1.80 (m, 4H), 1.80-1.10 (m, 16H), and 0.88 (t, *J* = 6.6 Hz, 3H). ^{13}C NMR ($CDCl_3$, 75 MHz): δ 176.5, 169.6, 130.4, 130.0, 128.3, 128.0, 50.7, 34.4, 31.7, 29.9, 29.5, 29.4, 27.4, 27.3, 25.8, 22.7, and 14.2. MS (ESI$^-$): calcd for $C_{21}H_{36}NO_6S$: 430.23 [M-H]$^-$; found: 430.56.

Linoleoyl AP3: The title compound was synthesized using the general method with linoleic acid (111.0 mg, 0.396 mmol), TBTU (133.6 mg, 0.416 mmol), triethylamine (88.2 mg, 0.871 mmol), and racemic 2-amino-3-phosphonopropanoic acid (45.5 mg, 0.269 mmol) as starting materials and acetonitrile/DMF (10 ml/1.5 ml) as solvents. The reaction mixture was stirred overnight at rt, concentrated, and purified using preparative LC (eluent: B:A: from 15:85 to 100:0). The fractions were combined, diluted with water (10 ml), and acidified with 2M HCl to about pH 2–3, then extracted with ethyl acetate 25 ml × 3. The organic layers were combined and concentrated to give to the title product (92.4 mg, 54%). ^{1}H NMR ($CDCl_3$, 300 MHz): δ 10.7 (br s, 3H), 7.49 (br s, 1H), 5.40-5.24 (m, 4H), 4.87-4.72 (m, 1H), 2.75 (t, *J* = 6.0 Hz, 2H), 2.70-2.10 (m, 4H), 2.10-1.92 (m, 4H), 1.67-1.48 (m, 2H), 1.48-1.10 (m, 14H), and 0.88 (t, *J* = 6.9 Hz, 3H). ^{13}C NMR ($CDCl_3$, 75 MHz): δ 176.4, 173.7, 130.4, 130.0, 128.2, 128.0, 48.5, 36.0, 31.7, 29.9, 29.6, 29.5, 29.46, 27.4, 27.3, 25.8, 25.7, 22.7, and 14.2. MS (ESI$^-$): calcd for $C_{21}H_{37}NO_6P$: 430.24 [M-H]$^-$; found: 430.45.

Pinoleoyl glycine: The title compound was synthesized using a similar method as the general method with pinolenic acid (14.9 mg, 0.0535 mmol), TBTU (20.6 mg, 0.0640 mmol), diisopropylethylamine (27.7 mg, 0.214 mmol), and glycine (4.8 mg, 0.0640 mmol) as starting materials and acetonitrile/DMSO (1.0 ml/0.2 ml) as solvents. The reaction mixture was stirred overnight at rt, concentrated, and purified using preparative LC (eluent: B:A: from 35:65 to 100:0). The fractions were combined and lyophilized to give the title compound (4.9 mg, 27%). ^{1}H NMR ($CDCl_3$, 300 MHz): δ 6.78 (t, *J* = 5.4 Hz, 1H), 5.90-5.68 (m, 6H), 4.42 (d, *J* = 5.4 Hz, 2H), 3.19 (t, *J* = 6.0 Hz, 2H), 2.69 (t, *J* = 7.5 Hz, 2H), 2.58-2.40 (m, 8H), 2.19-2.05 (m, 2H), 1.85-1.63 (m, 6H), and 1.31 (t, *J* = 6.9 Hz, 3H). ^{13}C NMR ($CDCl_3$, 75 MHz): δ 174.4, 173.1, 130.5, 129.4, 129.0, 128.8, 127.9, 42.0, 35.8, 31.7, 29.5, 27.45, 27.42, 27.37, 26.8, 25.9, 25.6, 22.7, and 14.2. MS (ESI$^-$): calcd for $C_{20}H_{32}NO_3$: 334.24 [M-H]$^-$; found: 334.55.

Pinoleoyl taurine: The title compound was synthesized using a similar method described for the synthesis of pinolenic glycine with pinolenic acid (14.9 mg, 0.0535 mmol), TBTU (20.6 mg, 0.0640 mmol), diisopropylethylamine (27.7 mg, 0.214 mmol), and

taurine (8.0 mg, 0.064 mmol) as starting materials and acetonitrile (2.0 ml) as solvent. The reaction mixture was stirred overnight at rt, filtered, and purified using preparative LC (eluent: B:A: from 15:85 to 90:10). The fractions were combined and lyophilized. To the solid, which was probably an ammonium salt, 1 ml of water was added. The pH value of the solution was adjusted to about 2–3 using 2M HCl. The solution was extracted with ethyl acetate 1.5 ml × 4. The organic layer was concentrated to give the title compound (17.0 mg, 82%). ^{1}H NMR ($CDCl_3$, 300 MHz): δ 8.28 (br s, 1H), 6.73 (br s, 1H), 5.50-5.19 (m, 6H), 3.90-3.55 (m, 2H), 3.32-3.00 (m, 2H), 2.76 (t, *J* = 5.7 Hz, 2H), 2.62-2.28 (m, 2H), 2.16-1.96 (m, 8H), 1.80-1.55 (m, 2H), 1.40-1.21 (m, 6H), and 0.88 (t, *J* = 6.9 Hz, 3H). ^{13}C NMR ($CDCl_3$, 75 MHz): δ 177.2, 130.8, 130.5, 129.3, 128.9, 128.5, 127.9, 49.7, 37.1, 34.8, 31.6, 29.5, 27.5, 27.38, 27.36, 26.8, 25.94, 25.87, 22.7, and 14.2. MS (ESI^-): calcd for $C_{20}H_{34}NO_4S$: 384.22 $[M-H]^-$; found: 384.47.

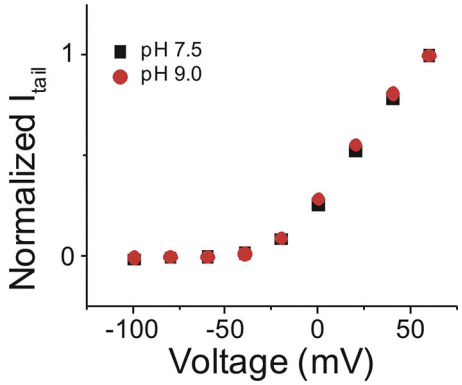

Figure S1. **Current versus voltage relationship between pH 7.5 and pH 9.0.** Current–voltage relationship of I_{Ks} channel in pH 7.5 (black squares; mean ± SEM; *n* = 4) and pH 9.0 (red circles; mean ± SEM; *n* = 4).

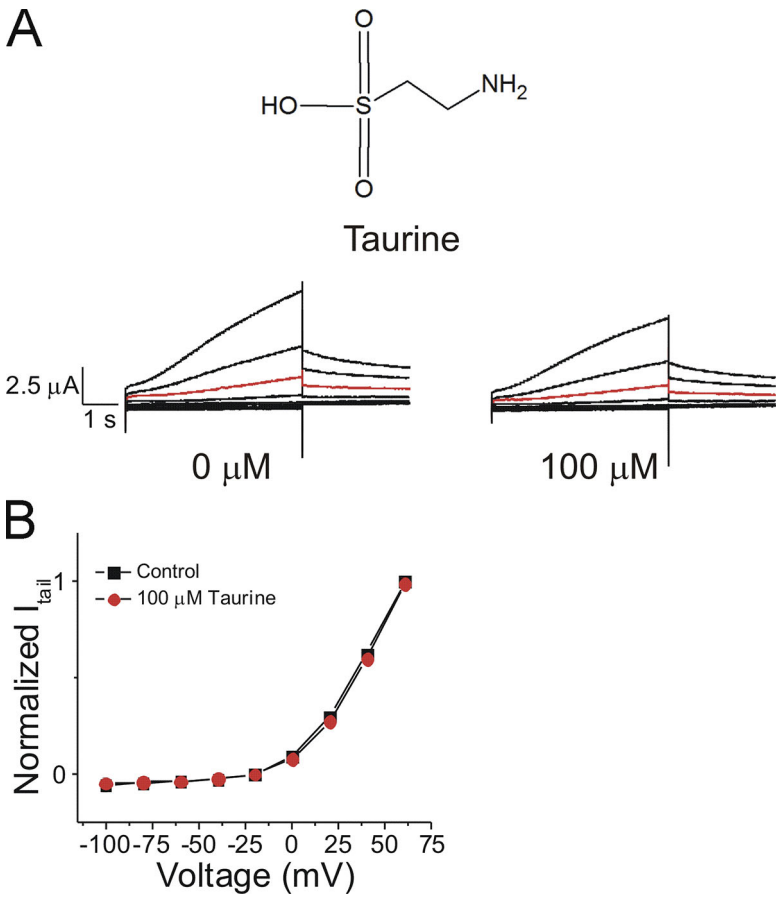

Figure S2. **Reduction of I_{Ks} current by the application of DHA taurine is not intrinsically related to the taurine head group alone. (A)** Structure of taurine and raw current traces measured in 0 µM taurine (left) and 100 µM taurine (right). Red trace shows currents at 20 mV for visualization of no effects of taurine on the voltage dependence. **(B)** Current versus voltage relationship in control (0 µM taurine) and following the addition of 100 µM taurine (mean ± SEM; *n* = 4).

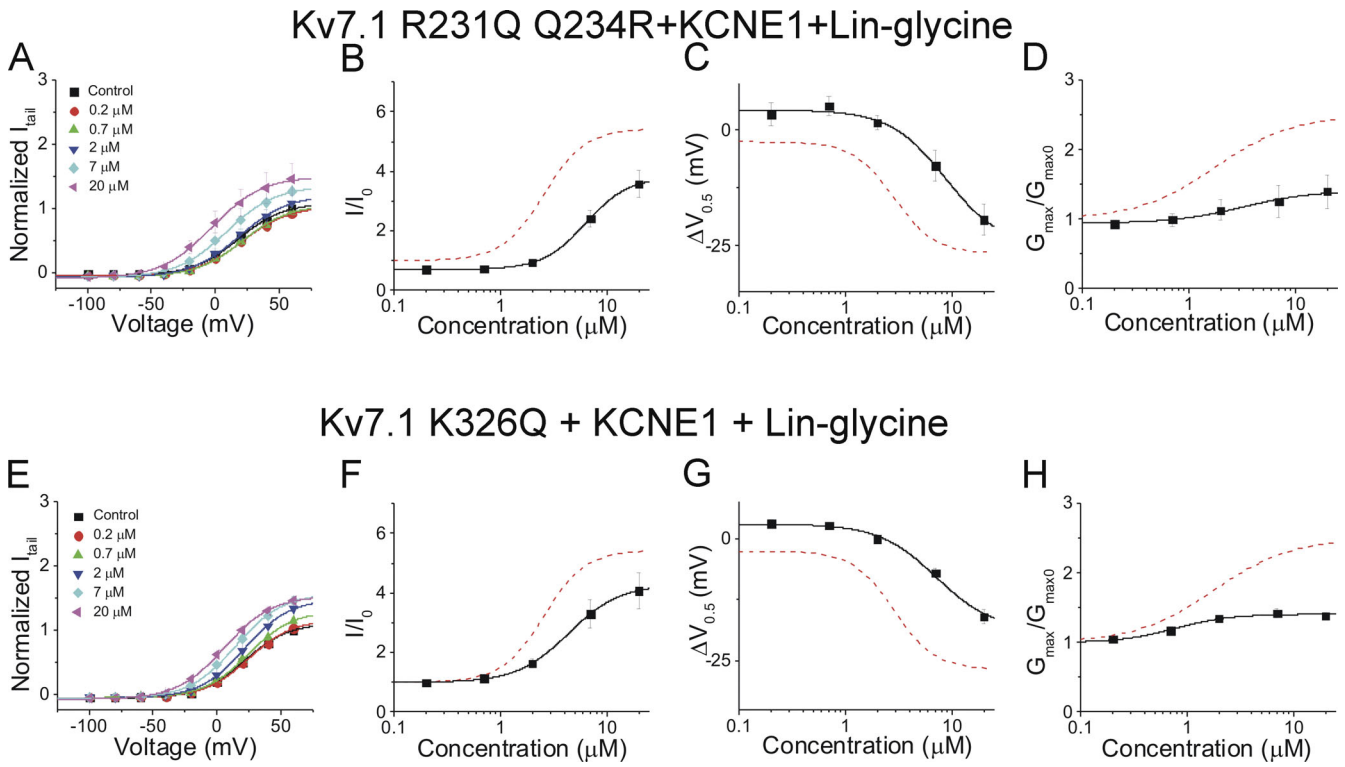

Figure S3. **Residues in the voltage sensor and pore are important for electrostatic activation of the cardiac I_{Ks} channel. (A)** Current–voltage relationship for Kv7.1 R231Q Q234R + KCNE1 with the application of lin-glycine (mean ± SEM; n = 4). **(B-D)** Dose-dependent effects of lin-glycine on Kv7.1 R231Q Q234R + KCNE1 (black squares) and the wild- type I_{Ks} channel (red dashed line) on (B) I/I_0, (C) $\Delta V_{0.5}$, and (D) G_{max}. **(E)** Current-voltage relationship for Kv7.1 K326Q + KCNE1 with the application of lin-glycine (mean ± SEM; n = 4). **(F-H)** Dose-dependent effects of lin-glycine on Kv7.1 K326Q + KCNE1 (black squares) and the wild-type I_{Ks} channel (red dashed line) on (F) I/I_0, (G) $\Delta V_{0.5}$, (H) G_{max}.

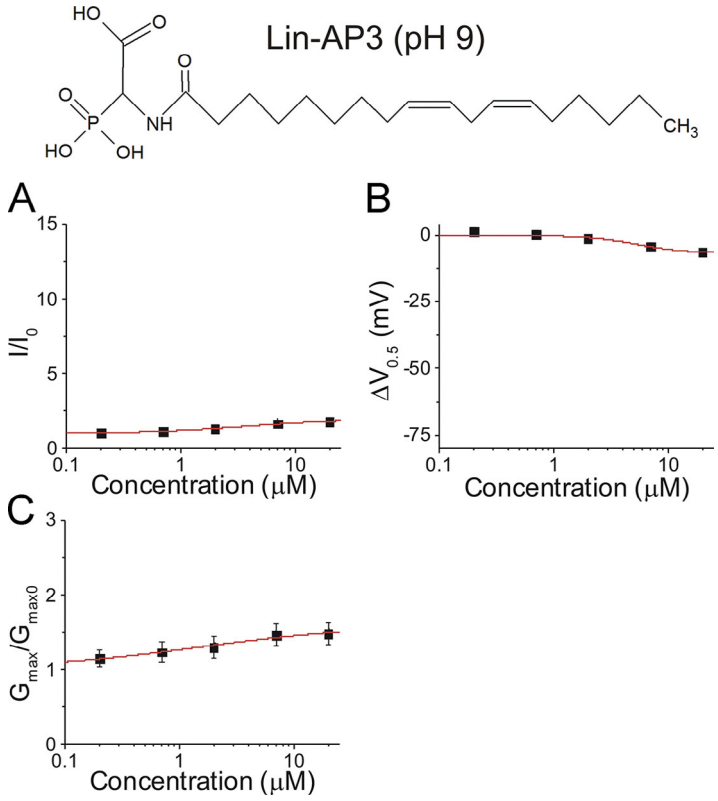

Figure S4. **Effects of lin-AP3 on I_{Ks} activation at pH 9.0. (A-C)** Dose-dependent effects of lin-AP3 on (A) I_{Ks} current (I/I_0), (B) I_{Ks} voltage dependence ($\Delta V_{0.5}$), and (C) I_{Ks} G_{max} at pH 9.0 (mean ± SEM at maximal concentration; *n* = 3).